Biochemical Society Transactions (2023) **51** 2041–2059
https://doi.org/10.1042/BST20221246

PORTLAND PRESS

Review Article

Insights into protein structure using cryogenic light microscopy

Hisham Mazal[1,2], Franz-Ferdinand Wieser[1,2,3] and Vahid Sandoghdar[1,2,3]

[1]Max Planck Institute for the Science of Light, 91058 Erlangen, Germany; [2]Max-Planck-Zentrum für Physik und Medizin, 91058 Erlangen, Germany; [3]Friedrich-Alexander University of Erlangen-Nürnberg, 91058 Erlangen, Germany

Correspondence: Vahid Sandoghdar (vahid.sandoghdar@mpl.mpg.de) or Hisham Mazal (Hisham.mazal@mpl.mpg.de)

Fluorescence microscopy has witnessed many clever innovations in the last two decades, leading to new methods such as structured illumination and super-resolution microscopies. The attainable resolution in biological samples is, however, ultimately limited by residual motion within the sample or in the microscope setup. Thus, such experiments are typically performed on chemically fixed samples. Cryogenic light microscopy (Cryo-LM) has been investigated as an alternative, drawing on various preservation techniques developed for cryogenic electron microscopy (Cryo-EM). Moreover, this approach offers a powerful platform for correlative microscopy. Another key advantage of Cryo-LM is the strong reduction in photobleaching at low temperatures, facilitating the collection of orders of magnitude more photons from a single fluorophore. This results in much higher localization precision, leading to Angstrom resolution. In this review, we discuss the general development and progress of Cryo-LM with an emphasis on its application in harnessing structural information on proteins and protein complexes.

Introduction

'In the drama of life on a molecular scale, proteins are where the action is' [1]. Proteins adopt complicated three-dimensional (3D) structures, and assemble into homogenous or heterogenous quaternary structures, ranging from small cellular components up to large assemblies such as viruses. Their 3D arrangement is a part of their dynamic mechanisms of action, governing and orchestrating every aspect of cellular physiology in both health and disease [2–5]. As such, understanding their structure and function has been a major focus in molecular biology. X-ray crystallography and NMR spectroscopy have successfully been used for this purpose, albeit with limitations, especially when dealing with large and complex biological macromolecules [6–12]. More recently, cryogenic electron microscopy (Cryo-EM) has emerged as a revolutionary method, allowing the determination of near-atomic and even atomic resolution structures of isolated macromolecules [13–17] (see Figure 1). The low contrast in this method, however, brings about challenges in identifying individual proteins and target molecules, thus, compromising the quality of attainable structural information in a native cell membrane [18–20], or identifying target molecules *in situ* [21,22].

Fluorescence microscopy has been instrumental in studying cellular and sub-cellular structures because it provides molecular specificity. Breakthroughs in single-molecule fluorescence detection [23,24] and manipulation of excitation beams have propelled the super-resolution (SR) era in optical microscopy, enabling investigations at the nanometer scale [25–28,36–41]. A hallmark of single-molecule fluorescence microscopy is the spatial localization of single molecules beyond the diffraction limit of light [29–31]. Here, one finds the position of each fluorophore by determining the center of its diffraction-limited point-spread function (PSF) with a precision that is dictated by the available signal-to-noise ratio (SNR) (see Figure 2A,B) [32–35]. Hence, a key notion in single-molecule localization microscopy (SMLM) [31] is the ability to turn individual fluorophores on and off. One game-changing approach has been to exploit photo-switchable dyes [25–27,42–47]. Although the attainable

Received: 26 August 2023
Revised: 13 November 2023
Accepted: 14 November 2023

Version of Record published:
28 November 2023

PORTLAND PRESS

Biochemical Society Transactions (2023) **51** 2041–2059
https://doi.org/10.1042/BST20221246

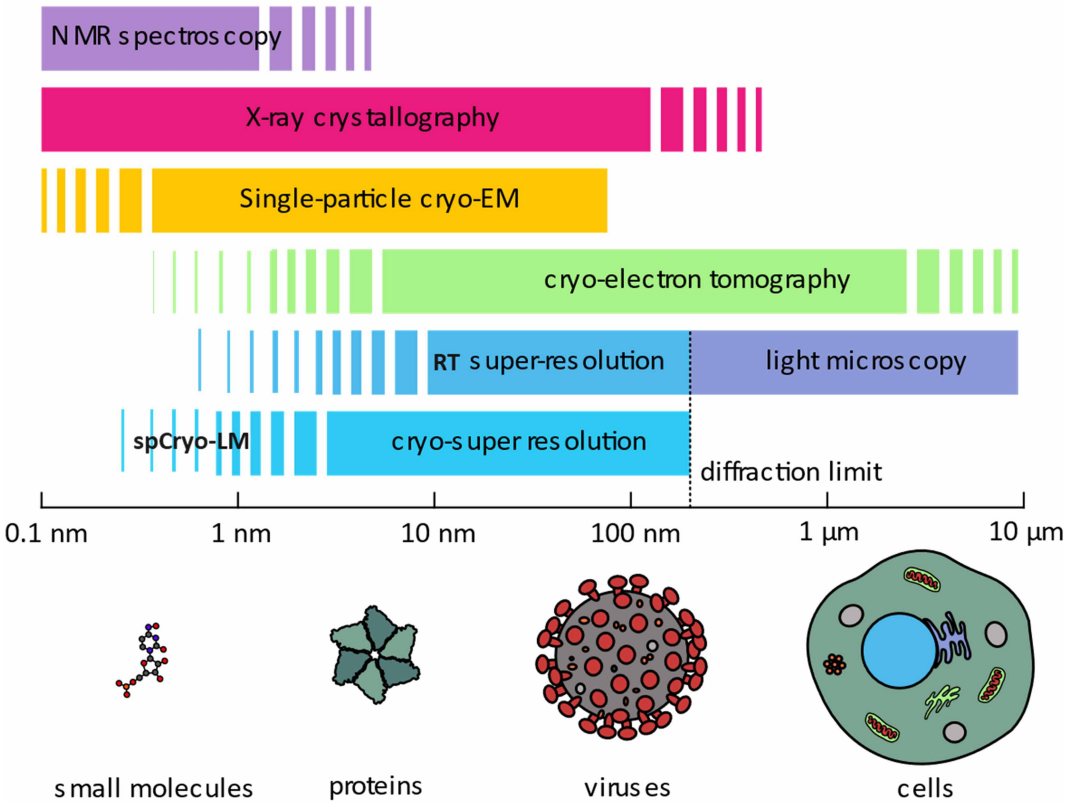

Figure 1. An overview of the resolving capability of different methods for studies in structural biology.
Different methods have been developed to investigate biological structures at various scales, ranging from a few Angstroms (small molecules) up to µm scales (cellular structures), not to scale. Light microscopy is unique in its wide coverage of scales, spanning from the Angstrom scale up to the millimeter scale.

resolution in SMLM is theoretically unlimited, in practice it usually does not fair better than 10 nm. First, photobleaching constrains the number of detectable photons, thus limiting the SNR (Figure 2B,C) [32,33,48–53]. Second, Nyquist's sampling theorem and the practical restrictions in labeling density pose a constraint on the achievable resolution [25,54–58]. Nevertheless, there has been a steady push to reach molecular and sub-molecular optical resolution [59–65], bridging the gap between light microscopy and electron microscopy (see Figure 1). These developments are very promising as they promise to shed light on the structure of biomolecules, especially proteins, at high spatial resolution. However, achieving this level of resolution requires a remarkably high degree of mechanical stability against thermal molecular jitter as well as instrumental vibrations and drifts, which has been tamed at room temperature (RT) only through chemical fixation or expansion. To minimize the risk of perturbations in the molecular structure of the sample, scientists have turned to cryogenic measurements, which are known to be compatible with near-native state preservation [66–68]. In this article, we review these efforts with an emphasis on their use in the analysis of proteins and protein complexes.

Cryogenic light microscopy (Cryo-LM)

Some of the first studies of protein conformational dynamics, in particular the structures underlying their potential energy surface, came from spectroscopic measurements at cryogenic temperatures (CTs) [70–83]. This was done by exploiting the narrowed spectrum of chromophores bound to proteins at low temperatures and following their spectral fluctuations as a function of time. High-resolution spectroscopy of single proteins, for instance, has revealed the dynamics of hydrogen bonds in cofactor binding sites [84]. The advantages of fluorescence studies at CT also gave way to the first single-molecule detection and high-resolution spectroscopy [85,86] as well as the first demonstrations of SR microscopy through spectral selection and localization of individual molecules [30,31,59].

Biochemical Society Transactions (2023) **51** 2041–2059
https://doi.org/10.1042/BST20221246

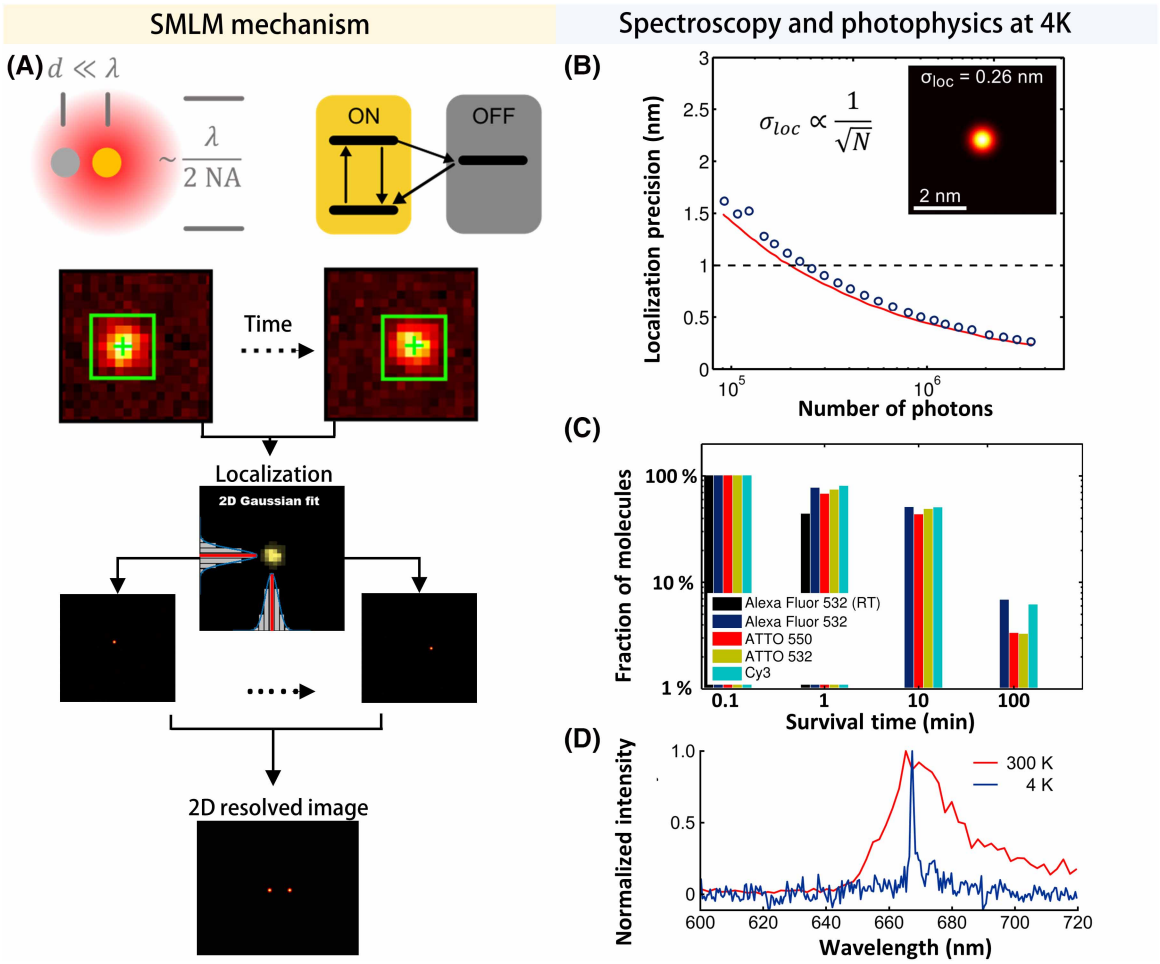

Figure 2. Principle of single-molecule super-resolution microscopy and the advantages of cryogenic operation.
(**A**) In SR microscopy based on single-molecule localization, individual fluorescent molecules located within a distance (d) below the diffraction limit of light (λ/2 NA), where λ is the wavelength and NA is the numerical aperture of the objective lens, are imaged one at a time. This process is facilitated by the stochastic transition of the fluorophores from the emissive state (ON) into the dark state (OFF). The PSF of each molecule is then fed into a localization algorithm, such as a 2D Gaussian model, to determine their coordinates with a precision better than the diffraction limit of light. A 2D super-resolved image is typically reconstructed from thousands of localization events [25]. (**B**) Localization precision (σ_{loc}) of a single Alexa Fluor 532 molecule at cryogenic temperatures as a function of the number of photons (N). The data represent the standard error of the mean of accumulated localization events. The red line is a theoretical curve based on Ref [32]. The fit to the model shows high localization precision on the order of 2.6 Angstroms (limited by drift correction). (**C**) Cumulative histogram of the survival times for different fluorophores at 4 K compared with Alexa 532 at RT under equivalent illumination conditions. It is evident that photostability is 2–3 orders of magnitude higher at 4 K compared with RT. (**D**) Comparison of a single-molecule emission spectrum (ATTO647N) at RT and 4 K, measured in our laboratory. A close to 10-fold reduction in the linewidth is achieved in the latter case. Panels **B**–**C** adapted from Ref. [69] with permission; copyright 2013 SPIE.

Cryogenic measurements offer two major advantages over RT imaging. First, the superior sample preservation strongly reduces thermal fluctuations and allows spectroscopy and microscopy at very high spectral and spatial resolutions [66,74,84,87–90] (Figure 2D, the data were measured in our laboratory). The second advantage is that photochemistry is considerably slowed down, leading to about three orders of magnitude more emitted photons from a fluorophore than at RT (Figure 2B,C) [69,91–93]. Together with the great asset of specific fluorescence labeling, these features promote the development of cryogenic light microscopy (Cryo-LM) for correlative imaging with other cutting-edge techniques such as Cryo-EM [94–101] that suffer from less

Biochemical Society Transactions (2023) **51** 2041–2059
https://doi.org/10.1042/BST20221246

specificity. Here, a biological sample is preserved in its near-native state via shock-freezing or high-pressure freezing, where the fast cooling rate preserves water molecules in their random structure, generating amorphous ice (vitreous ice) [67,102–105], which keeps the sample hydrated. This is not the case for the more natural crystalline form of ice, leading to morphological damages to the molecular structure of the sample [67,106]. To maintain vitreous ice, the sample must be kept below the devitrification point which is ∼136 K [104].

The simplest way to perform fluorescence microscopy at low temperatures is to cool the sample under ambient pressure [107–109] (Figure 3A). For example, a cold finger can be immersed in a liquid nitrogen (LN_2) reservoir while maintaining the local surroundings with cold dry nitrogen (cN_2) atmosphere to prevent ice condensation. This method is easy to use because the sample can be placed under a conventional RT microscope, but the arrangement is prone to condensation and contaminations, both on the sample itself and on the microscope objective. Besides, large temperature variations can give rise to aberrations in the objective. In addition, the setup suffers from severe drifts, which are especially troublesome if one is interested in longer acquisition time [100,110]. Alternatively, enclosed chambers can be used, while the microscope objective sits outside a window to the sample chamber [69,93,99,102] (Figure 3B). Here the sample can be maintained under an N_2 atmosphere or high vacuum. The latter allows temperatures as low as 4 K by operating with liquid helium (LHe) and offer better performance in terms of sample preservation and mechanical stability [69,93,101,102]. The third arrangement depicted in Figure 3C includes the imaging optics inside the cryostat under vacuum or LHe condition [60,88,111,112]. While all three schemes can use air objectives with numerical apertures (NA) as high as ∼0.9, the last alternative has the advantage of being compatible with using optics with NA > 1 based on solid-immersion lens (SIL) technology [113,114].

For correlative Cryo-LM and Cryo-EM studies, imaging is usually pursued in a sequential fashion. In this process, target-labeled biomolecules are initially mapped using a fluorescent microscope, offering highly sensitive and specific information about their locations. These maps are then employed as references to guide electron microscopy on the same sample, enabling the acquisition of greater informational detail and resolution for a desired region of interest with higher efficiency [94,95,99,110]. For example, Briegel et al. [116] used such an approach to identify the location of chemoreceptor arrays in *C. crescentus* bacterial cell, which were then mapped at higher resolution using cryogenic electron tomography (Cryo-ET). In this genre of applications, one might be satisfied with the diffraction-limited resolution of light microscopy.

Cryogenic fluorescence microscopy lends itself particularly well for achieving SR. As a result, several groups have explored this approach on sub-cellular structures (Figure 4A–D). A detailed report on this topic can be

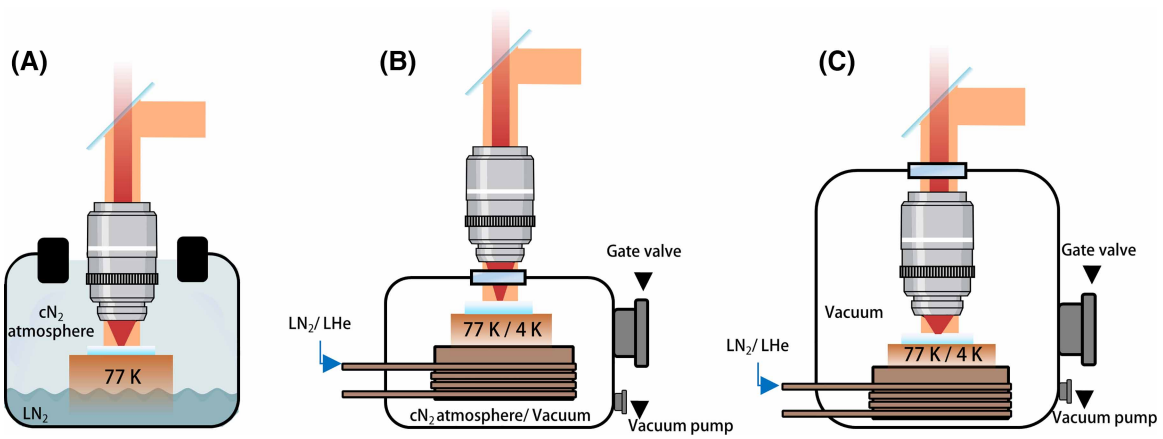

Figure 3. Schematic overview of different cryogenic light microscopes.

(**A**) An open-atmosphere LN_2 optical microscope. These types of setups generally allow easy sample exchange but suffer from condensations as well as severe mechanical and thermal drift. (**B**) A closed high-vacuum/cold N_2 atmosphere (cN_2) chamber with a cooling stage. The microscope objective is placed outside the sample chamber. (**C**) A cryostat consisting of a closed high-vacuum optical microscope and a microscope objective placed inside the chamber. This setup showcases exceptional mechanical and thermal stability. Both arrangements **B** and **C**, allows sample exchange in and out of the microscope via a proper cryo-shuttle [102,115].

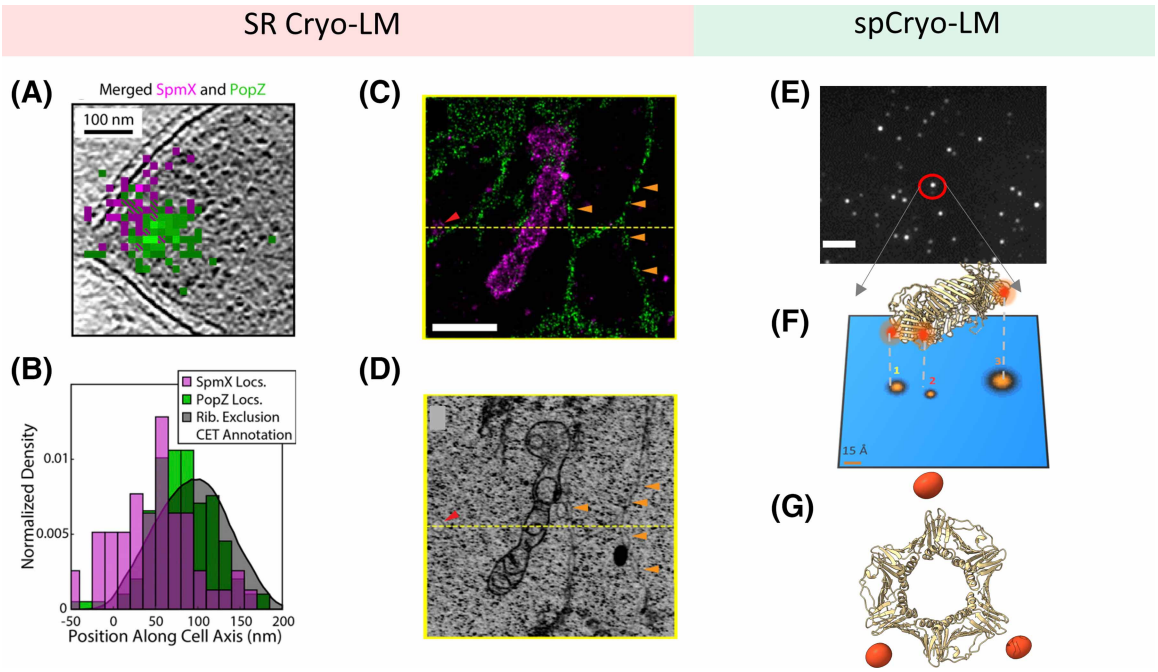

Figure 4. Overview of different super-resolution cryogenic light microscopes and their application to biological samples.

(**A** and **B**) Cryo-PALM imaging super-resolves the spatial locations of two model proteins within a frozen-hydrated bacterial cell (PopZ and SpmX, purple and green color, respectively) conjugated to a photo-switchable fluorescent protein (PamKate). This approach combines near-native sample preservation and high photostability of the fluorescent molecules to demonstrate the accurate identification and localization of the two proteins with respect to the bacterial axis with a high spatial precision of 9 nm. This identification was later successfully correlated and validated with the images obtained from Cryo-ET [107]. Panel **A**–**B** adapted from Reference [107] with permission; copyright 2020 PNAS. (**C** and **D**) A near-native whole vitrified cell was imaged at LHe temperature to take advantage of the enhanced photophysics and stability of fluorescent proteins or organic molecules. This approach allowed for the resolution of 3D spatial information and the distribution of protein markers within their ultrastructural context. For instance, by using the highly sensitive localization information of the (ER3-green color), ER protein marker and the outer membrane protein marker of the mitochondria (TOMM20-purple color) (**C**), together with detailed cellular images obtained from FIB-SEM (**D**), a variety of unexpected sphere-shaped ultrastructures were revealed [102]. Orange arrows indicate ER varicosities, and red arrow indicate TOMM20-positive vesicles. The scale bar is 1 μm. Panel **C**–**D** adapted from Reference [102] with permission; copyright 2020 Science. (**E**) Wide-field image of labeled single proteins (scale bar: 5 μm). This method demonstrates spCryo-LM, where the density is chosen to be low enough to only have one single protein or protein complex within the diffraction limit of the optical system. (**F** and **G**) This method able to resolve the configuration of protein complexes with Angstrom-scale resolution (discussed in "Single-particle cryogenic light microscopy" section). The figure depicts a homotrimer of protein PCNA (PDB: 1AXC), where each domain is labeled specifically at the N-termini side with a single fluorophore. The 2D resolve image demonstrate a single projection of the protein in the sample localized with Angstrom scale precision. 2D projections are combined to arrive at the 3D arrangement of the fluorophore on the protein [131].

found in recent review articles [117,118]. In Table 1, we present an overview of some of the setups used in these efforts with an emphasis on applications of SR microscopy and vitrified samples. In general, the obtained resolution has remained comparable with that achieved at RT, i.e. in the order of 10–150 nm (Figure 1) [102,107–109,117,119,120]. Beside the low NA being used in such microscopes, one can identify three main reasons for the limited resolution: (1) Photophysics at CT, especially photo-switching and photobleaching properties of fluorophores, are not well understood or are insufficient [117,118]. For example, in the case of fluorescent proteins the switching efficiency is reported to be diminished [109,120–124]. (2) The laser power has to be kept low to avoid sample devitrification [120,125,126], leading to low signals. (3) Importantly, most studies have been performed in densely labeled environments, which might hinder one from localizing a single

Biochemical Society Transactions (2023) **51** 2041–2059
https://doi.org/10.1042/BST20221246

Table 1 Cryogenic temperature super-resolution fluorescence microscopy of biological samples

Paper	SR method	Temperature [K]	Condition	Objective	Precision/ resolution [x,y]	Precision/ resolution [z]	Remarks
[109]	SMLM (Cryo-PALM)	LN_2	cN_2	60×, 0.75 NA	170 nm	-	Using Cryostage^2
[108]	SMLM (Spontaneous blinking)	LN_2	cN_2	63×, 0.75 NA	125 nm	-	Using Cryostage^2
[132]	SMLM (Spontaneous blinking)	LHe	Vacuum	100×, 0.75 NA	~7 Å	-	1 nm accuracy spCryo-LM (preserved in hydrophilic polymer)
[124]	SMLM (Cryo-PALM)	LN_2	cN_2	100×, 0.8 NA	~ 8 nm (Single molecules)	40 nm (Single molecules)	75 nm in 3D
[133]	SMLM (Cryo-PALM)	LN_2	cN_2	100×, 1.3 NA	~35 nm	-	High NA using cryofluid
[60,131]	SMLM (Spontaneous blinking)	LHe	Vacuum	100×, 0.9–0.95 NA	4–8 Å	-	5–7 Å in 3D, spCryo-LM (preserved in hydrophilic polymer)
[123]	SMLM (Cryo-PALM)	LN_2	cN_2	100×, 0.9 NA	9 nm	-	
[134]	SMLM (Cryo-PALM)	LN_2	cN_2	100×, 0.8 NA	17 nm		Exceptional stability in an open atmosphere setup
[135]	Spectrum	LHe	Vacuum	Cryo-objective mirrors	1 nm	11 nm	spCryo-LM
[119]	Super-resolution optical fluctuation imaging (SOFI)	LN_2	cN_2	50×, 0.9 NA	135 nm		
[120]	SMLM (Cryo-PALM)	LN_2	cN_2	100×, 0.75 NA	30 nm		
[136]	SMLM Stochastic optical reconstruction microscopy (STORM)	LN_2	cN_2	100×, 0.55 NA with SIL	12 nm		
[107]	SMLM (Cryo-PALM)	LN_2	cN_2	100×, 0.9 NA	9 nm	-	Registration error with Cryo-TEM ~30 nm
[102]	Cryogenic SMLM & SIM	LHe	Vacuum	100×, 0.85 NA	~2–5 nm	~25–100 nm	Registration error with Cryo-FIB-SEM ~40 nm
[137]	Cryogenic 3D-SIM	LN_2	cN_2	100×, 0.9 NA	210 nm	640 nm	Obtained at 488 nm laser excitation
[138]	Cryogenic confocal microscope	LN_2	cN_2	100×, 0.75 NA	290 nm	1150 nm	ZEISS LSM 900 confocal microscope equipped with an Airyscan 2 detector
[139]	Cryogenic super-resolution radial fluctuations (Cryo-SRRF)	LN_2	cN_2	0.9 NA	~100–200 nm	-	EM Cryo CLEM (Leica Microsystems)

fluorophore with high precision. For example, in Ref. [107] cryogenic photo-activated localization microscopy (Cryo-PALM) was employed using an open atmosphere cryo-stage to determine the spatial location of multiple model proteins with respect to axis of a frozen-hydrated bacterial cell. This yielded ~10 nm-scale localization precision (Figure 4A,B and Table 1), which was limited by mechanical stability and low laser illumination for fluorescent protein photo-activation. In another recent work [102], the conditions on the laser power and sample stability were improved by mounting the sample on a sapphire disc rather than a carbon film (transmission electron microscope grids). In addition, an enclosed setup operating at LHe temperature provided better mechanical and thermal stability, and it allowed the researchers to exploit the longer dark state of fluorescent protein and fluorescent molecules at high-vacuum and 8 K, reaching a better localization precision (Figure 4C, D and Table 1). A combination of multiple SR methods such as structured illumination microscopy (SIM) and SMLM was employed to super-resolve large cellular structures such as mitochondria and ER in whole vitrified eukaryotic cells with high specificity and sensitivity. Regarding the choice of the coolant medium, LHe is

advantageous over LN_2 as it assures more stable coolant flow and less bubbling although the cost of LHe is much higher. Although LHe provides a significant cryoprotection against radiation damage in electron microscopy [90], its importance for the preservation of biological samples has not been clarified [127,128]. In general, LHe should be able to reduce the thermal jitter of biomolecules more than LN_2. In our laboratory, we opt for LHe due to its better performance in terms of spectroscopy and photophysics [88,102,129,130]. However, a quantitative investigation and characterization of the photophysics at various temperatures, with and without vacuum has not yet been fully established.

Single-particle cryogenic light microscopy (spCryo-LM)

A fundamental challenge in SR microscopy is achieving a very high-density labeling to satisfy the Nyquist–Shannon sampling theorem [57]. For example, to be able to image all parts of a dense two-dimensional (2D) structure at a resolution of a few tens of nanometers, several thousands of fluorophores must be localized within a diffraction-limited spot. For a sample that is extended in the third dimension, the number scales accordingly, making it a daunting task to resolve cellular structures with a true resolution in the order of a few tens of nm. Even if this were to be realizable, one would then require a sufficiently performant photo-activation to ensure that only one fluorophore is on at any given time in order to achieve high localization precision and structural resolution. Nevertheless, SR Cryo-LM can be exploited to resolve the 3D configuration of isolated finite-sized nanostructures at Angstrom optical resolution. As depicted in Figure 4E–G, here one chooses a sparse coverage of the nanostructures to avoid having more than one per PSF. Moreover, each subdomain of interest is conjugated with a single fluorophore. If the number of subdomains is not too large, one can localize each fluorophore individually at Angstrom resolution, thus, deciphering the stoichiometry and assembly of the nanostructure at hand. We shall refer to this technique as single-particle cryogenic light microscopy (spCryo-LM), which we choose as the main focus of this review. Considering the recent emergence of this approach, the article remains somewhat biased on the work from own laboratory.

Photoblinking at 4 K

SMLM relies on mechanisms that allow one to image one molecule at a time. The pioneering works in RT SR microscopy used photo-activation of synthetic dyes [43] or fluorescent proteins [26,44,45]. In principle, the same techniques can also be used in spCryo-LM [60,131], but as mentioned earlier, knowledge of these phenomena at CT is still limited. In our laboratory, we have chosen to use naturally occurring stochastic photoblinking of organic dyes [25]. Fluorescence intermittency in these molecules has been extensively characterized at RT and has often been found to follow non-exponential probabilities. This behavior has been attributed to transitions to trapped states, which generation can depend on the environment of the surrounding material and temperature as well as the excitation wavelength and intensity. Despite several vigorous studies, many questions remain open in this field [143–150].

Investigations of photoblinking of organic molecules at low temperatures are scarce [151]. At LHe temperature, however, we find several blinking behaviors, such as exponential and power law for several conventional dyes (ATTO, Cy, Alexa) [130,152,153]. As a physical rule of thumb, one can argue that under ambient conditions transitions from the triplet state back to the ground state are typically mediated by collisions with singlet oxygen [151,154,155]. The abundance of oxygen ensures a fast fluorescence recovery and short off-times in this case. At low temperatures and in high vacuum, diffusion of singlet oxygen is reduced, leading to longer off-times, which is favorable for single-molecule localization microscopy.

In general, to resolve N fluorophores unambiguously within a diffraction-limited spot, we require an on–off ratio smaller than 1/N. In addition, the frame rate of the camera needs to be faster than the average off-time to minimize the probability of overlapping contributions from many molecules in a single image. It is not straightforward to predict the on- and off-times of fluorophores at CTs from their values in solution, and common strategies cannot be directly used to engineer them. Typically, the off-on ratio ranges between 5 to 30, and strongly depend on the nano-enviroment, as well as illumination power [131,152]. Different setups have reported spontaneous blinking at 4 K, but experiments operating at LN_2 and open atmosphere have not been successful in achieving high blinking ratios. As a result, they have been limited in the number of collection photons and the attainable localization precision [107,118]. Modulating the blinking behavior at CT is still not explored.

Biochemical Society Transactions (2023) **51** 2041–2059
https://doi.org/10.1042/BST20221246

Identification by brightness

The early work on spCryo-LM demonstrated co-localization of two organic fluorophores on a DNA backbone, reaching sub-nanometer accuracy [132]. The method was then extended to resolving two fluorophores bound to the C termini of the cytosolic GtCitA PAS protein domain and four fluorophores bound to the four biotin sites of single streptavidin molecules [60]. This first application of spCryo-LM reached the remarkable 3D resolution of 5 Angstrom for sites distanced by ∼2 nm (Figure 5A–E). This method was named cryogenic optical localization in 3D (COLD) [60]. Here, proteins were embedded in a hydrophilic polymer at LHe temperature and by exploiting the slow stochastic blinking of organic fluorophores, each was identified based on its intensity level (Figure 5A). In the most general case, the time traces are expected to show only N discrete jumps corresponding to the step-wise photoblinking of N identical fluorophore per particle. However, variations in orientation, local environment and quantum efficiency leads to 2^N combinations of the on/off-state signal levels. Individual molecules are addressed by sorting imaging frames that correspond to each of the N lowest levels and taking their average for localizing each level separately.

Upon the successful localization of the fluorophore positions conjugated to a target molecule, it is straightforward to generate the 2D resolved images, whereby a 2D Gaussian function is assigned to each localized fluorophore with a width given by the respective localization precision. Due to the 3D random orientations of individual proteins in the sample, a given structure gives rise to a wealth of 2D projections (Figure 5C). Assuming that all structures are intrinsically identical, one can follow a protocol similar to that used in single-particle reconstruction in electron microscopy [14,156]. Here the 2D resolved images are fed to a maximum-likelihood algorithm, which reconstructs the 3D structure in an iterative manner (Figure 5D,E). The reconstructed model can generally be improved by filtering the 2D data sets, for example, by filtering based on the localization precision (Figure 5B), number of photons, maximum/minimum resolved distance, number of polarization states, etc.

Upon successful co-localization and assignment of fluorophore positions within a particle, a quantitative value that estimates the quality of the model reconstruction can be obtained using the Fourier shell correlation (FSC) in 2D or in 3D [157,158]. FSC simply calculates the correlation between the two half data set reconstructions. The resolution is then determined by finding the point of intersection of the FSC curve with the curve of a resolution criterion, such as the half-bit criterion (Figure 6F) [159].

Identification by polarization

The intensity-based co-localization approach discussed above suffers from low yield because in most cases, the blinking traces are not sufficiently well resolved. A more robust and efficient scheme exploits polarization differences from individual fluorophores on a given particle, see Figure 5F–K [152], taking advantage of the fact that contrary to RT experiments, fluorophores do not rotate and possess fixed dipole orientations. Unlike fluorescence brightness, which is subject to temporal fluctuations due to transitions between nearby levels (Figure 5A), polarization angles can be separated more clearly, thus reducing errors in measurements (Figure 5G).

A simple method to measure the molecular orientation is to split the emitted light with a single polarizing beam splitter to two channels with orthogonal polarizations. The polarization in the image plane is then determined from the ratio of the intensities registered in the two channels, which yield an angular interval $\theta \in [0°, 90°]$ (Figure 5F,G). This approach, which was termed polarCOLD, was first demonstrated on DNA origami structures ranging from 6 nm up to 95 nm with high localization precision (Figure 5J,K) [152,153]. In Figure 4F, we present an example of a homotrimer protein complex PCNA labeled with three ATTO647N dyes at N-termini sites [131]. The three distinct populations of polarization trajectories were used to locate the three binding sites. A 2D resolved image was generated from each trajectory by clustering the localization of polarization populations separately. The resulting images were then used to solve the 3D information.

Despite the extended range in the polarization space, resolving larger numbers of labels per particle becomes increasingly challenging (low yield) because of the higher probabilities of several overlapping polarizations. Currently, we estimate that about six emitters per particle can be addressed comfortably based on the angular width of each polarization distribution [131]. Application of more sophisticated analysis methods, e.g. based on machine learning or imaging in 3D, promises to push this limit further. As another way to address this limitation, we reduced the labeling efficiency of the fluorophores such that the majority of the complexes contained 2–4 molecules per complex only. As an example, a protein disaggregation machine composed of six identical subunits, ClpB, was labeled at 50% labeling efficiency by attaching an ATTO647N dye specifically on its M

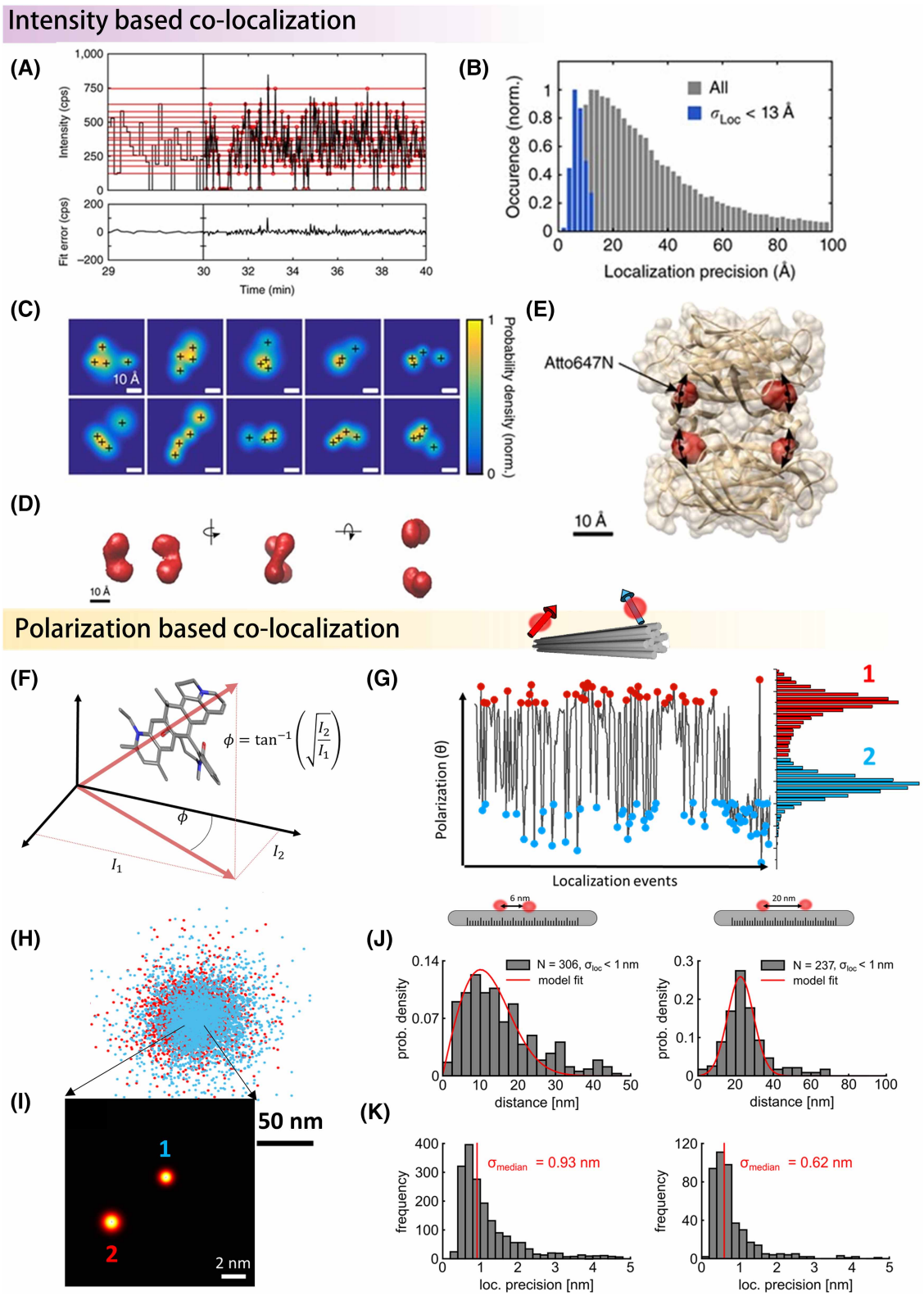

Figure 5. single-particle cryogenic super-resolution approaches. Part 1 of 2

(**A**) Intensity-based co-localization approach. Here, intensity levels in a blinking time trace are used to annotate and localize each fluorophore separately. The example depicts a time trace of four fluorophores on a streptavidin protein conjugated to four labeled biotin molecules. The time trace exhibits 2^4 distinct levels, which correspond to various combinations of the four

Biochemical Society Transactions (2023) **51** 2041–2059
https://doi.org/10.1042/BST20221246

Figure 5. single-particle cryogenic super-resolution approaches. Part 2 of 2

fluorophores due to their distinct local environments [60]. After fitting the data with a proper model, only the lowest four levels are utilized for annotating and localizing the fluorophores over time. (**B**) The overall localization precision is obtained from thousands of particles (gray color). The blue area highlights the molecules with high localization precision. (**C**) 2D resolved images obtained from localizing each identified fluorophore based on the intensity trace, showing different particles at different projections. By exploiting single-particle analysis algorithms borrowed from Cryo-EM, distinct 2D resolved projections (**C**) are reconstructed to reveal the 3D spatial configuration of the fluorophores (**D** and **E**, PDB: 1STP) [60]. (**F** and **G**) The second and more robust approach to fluorophore annotation involves exploiting their fixed dipole orientation at CT (**F**). The polarization time trace in (**G**) is obtained by measuring a DNA origami structure conjugated with two fluorophores at a fixed distance (see inset), and depict a short part of the on events cropped from a long trajectory. One finds two distinct populations of polarization, which reflect the appearance of the two fluorophores as they blink over time. By collecting all the raw localization events for each fluorophore separately, a 2D super-resolved image can be reconstructed (as shown in **I**, depicted in **H**). Employing this approach enables resolving variety of distances with sub-nanometer localization precision (**J**) [152]. The Inset depict the designed distance on a DNA origami substrate. The top histograms depict the distance distribution, and bottom histograms depict the localization precision, respectively (**K**). Panels **A–E** adapted from Ref. [60] with permission; copyright 2017 Nature Springer. Panels **G–K** adapted from Reference [152] with permission; copyright 2020 ACS photonics.

domain. Given the hexagonal symmetry of the structure, three distinct classes of configurations are expected (Figure 6A–C). To sort these various classes and to demonstrate the ability of this approach for studying heterogenous samples, a pipeline based on supervised template matching was implemented to classify each 2D projection (Figure 6C). Figure 6D–F displays the remarkable success of the method in identifying three different configurations within the same sample with high confidence. After solving their 3D structures separately, they were merged together to obtain the full 3D configuration of the six labeling sites on the ClpB protein and to decipher the symmetry of the protein complex at high resolution (Figure 6F,G) [131]. In the case of an unknown sample, this approach might require some prior knowledge on the number of monomers per molecule, which can be obtained from several biochemical assays such as native gel, gel chromatography or even simple negative stain electron microscopy.

Quantitative classification approaches have also been demonstrated in the field of single-particle SR microscopy at RT mainly assuming symmetric models and applied to large protein complexes such as the nuclear pore complex [160–165]. For example, Curd et al. [162] developed a pipeline that finds the symmetry of the protein complex based on a pairwise distance histogram. Heydarian et al. [166] used an all to all registration scheme to combine a classified projection into one average data set, which resolved the complete structure. However, this approach works mainly on a close to top view images, in case of 2D imaging approach. A 3D version of the same scheme was developed later which considers the information from the 3 coordinates x, y and z. This approach allows resolving particles with different orientations but it assumes a homogenous subset of the molecules, i.e. a single conformation. For example, this approach was recently applied to resolve several conformation of the PIEZO1 protein in a chemically fixed cell membrane [167]. We remark that the complexity of the orientation problem can be reduced significantly by confining the protein to a single orientation, e.g. via tethering to a surface such as DNA hybridization or similar approaches [168].

Future directions

Structural biology faces new challenges as it ventures into the native cellular environment targeting smaller proteins and their complexes. It is to be expected that all existing imaging spectroscopy methods continue to improve both on the hardware and the analysis sides, especially taking advantage of powerful machine learning algorithms. The Angstrom localization precision obtained in Cryo-LM already surpasses the fundamental resolution limit of fluorescence microscopy, which is posed by the physical size of the fluorophore rather than the laws of physics. It is, thus, interesting to develop fluorescent dyes with minimal extension. Moreover, design and synthesis of fluorophores with optimized switching capabilities at low temperature would strongly benefit Cryo-LM.

It is to be born in mind that the community of SR microscopy considers the individual fluorophores to be independent. While this is a reasonable assumption at distances larger than 10 nm and at RT [55], molecules can undergo coherent and incoherent dipole-dipole coupling at very small distances such that the locations of emission and absorption no longer coincide. This would smear the localization precision at the nanometer

Biochemical Society Transactions (2023) **51** 2041–2059
https://doi.org/10.1042/BST20221246

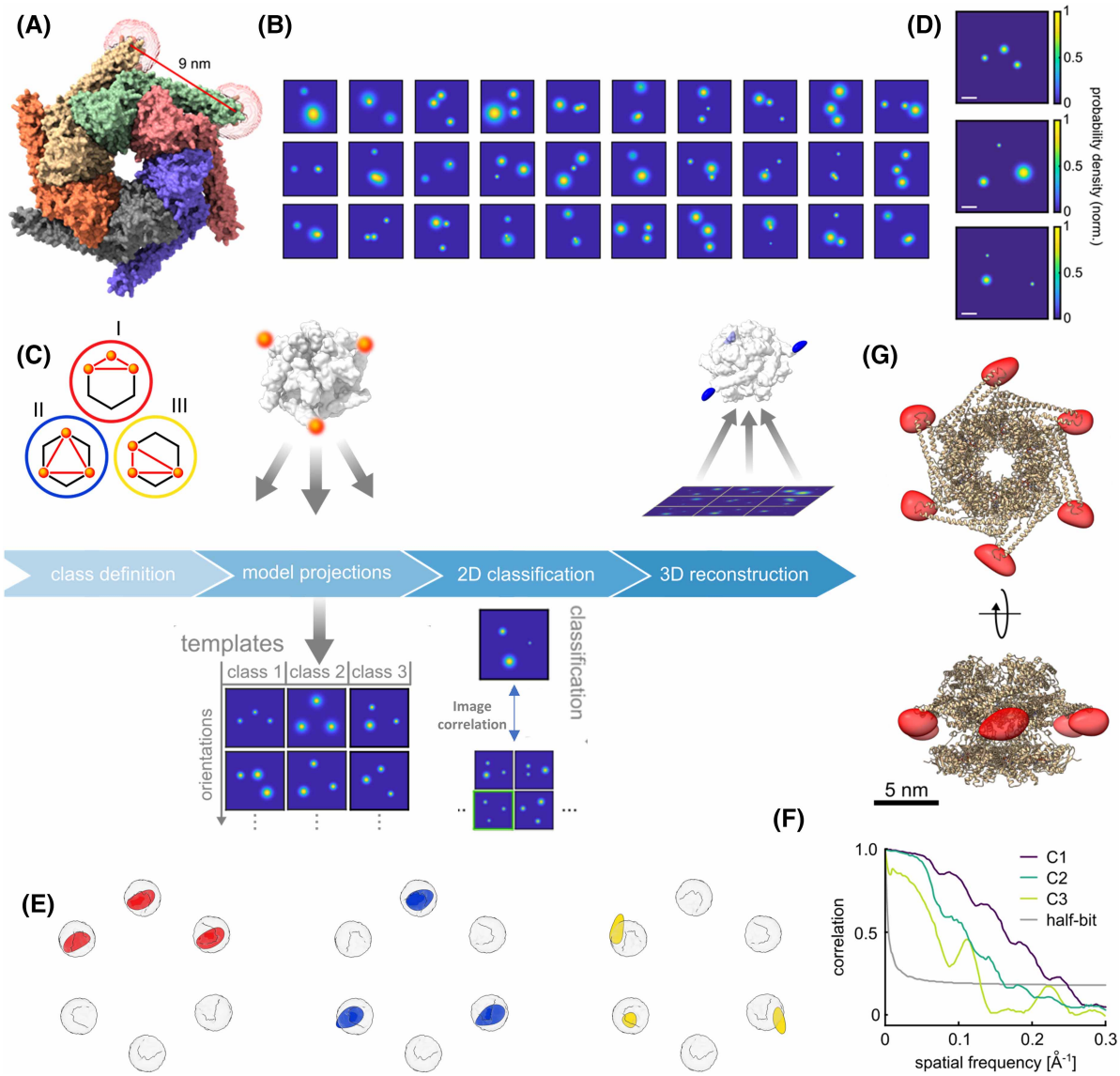

Figure 6. Single-particle classification and reconstruction in a model-system.

(**A**) Crystal structure of hexamer protein, ClpB (PDB: 1QVR). The labeling positions and the distance between them are marked. (**B**) 50% labeling efficiency of the protein inherently yields three different classes of different configurations and distances due to the C6 symmetry of the hexamer (**C**). (**B**) Examples of 2D super-resolved particle images in a 30 nm × 30 nm box with 0.15 nm pixel size emerge from the heterogeneous particles in the sample. (**C**) A strategic pipeline for classifying the images obtained in (**B**) to three classes. An approach based on template matching is employed here. Initially, an extensive library of images is generated for each class, encompassing all possible 3D orientations. Subsequently, each experimental image is cross-correlated with the image library of all classes. The experimental images are assigned to the class that yielded the highest correlation score. (**D**) A near-top view projection of each class. The images for each class are subsequently employed for separate 3D reconstruction. (**E**) The reconstructed fluorophores' positions (red, blue, yellow) align with their expected theoretical accessible volumes (gray spheres). (**F**) Fourier shell correlation curves of the reconstructed fluorophore volumes. The intersection with the half-bit criterion determines resolutions of 4.0, 7.9 and 6.4 Å, respectively. (**G**) By combining the partially resolved classes, a full structure can be resolved. Panels **D**, **E**, **F** and **G** adapted from Reference [131] with permission; copyright 2022 eLife.

Biochemical Society Transactions (2023) **51** 2041–2059
https://doi.org/10.1042/BST20221246

scale. The best known case of incoherent coupling is that of fluorescence resonant energy transfer (FRET), where energy is transferred from a donor molecule to an acceptor molecule at distances less than ∼10 nm [169]. It is important to keep in mind that the less known homoFRET can also take place between molecules of the same species. Moreover, as dephasing is reduced at CTs, coherent coupling between molecules can lead to the hybridization of the energy levels and again delocalize emission and absorption over the extent of the molecular ensemble [59]. So far, we have not confronted restrictions from such dipole-dipole couplings, but future studies are needed to quantify their role. Indeed, combination of Cryo-LM and cryogenic laser spectroscopy would provide more information about the nature of the coupling, which depends on the fluorophore orientation and distance much in analogy with the analysis of NMR spectra.

The currently achieved SNR and Angstrom precision of spCryo-LM is already capable of providing pivotal solutions for quantitative structural analysis of small proteins as well as large protein complexes and aggregates. In particular, crucial information about protein assembly such as configuration and symmetry as well as conformational changes can be obtained by labeling various domains. Moreover, protein–ligand interactions can be investigated by labeling ligand molecules such as biotin or ATP. Novel algorithms based on deep learning [170,171] also promise to increase the number of fluorescent molecules that can be identified per particle and will enhance the measurement yield by improving particle classification.

A specially promising line of study concerns the conformation and clustering states of membrane proteins in their native environment. Indeed, an estimated 20% of the human genome encodes membrane proteins and many of them are potential drug targets [172]. In current experiments in our laboratory, we vitrify and preserve biological samples via rapid freezing [67,173], allowing us to perform spCryo-LM on membrane proteins in their natural environment. As discussed previously, this approach has been successfully implemented in different types of microscopes [102,107,119,120] (see also Table 1). In this case, membranes can be prepared by cell unroofing or generation of cell-derived membrane vesicles [174,175]. Such investigations would ideally complement many existing techniques such X-ray crystallography, NMR, and Cryo-EM, which do not perform well on membrane proteins in their native environment, e.g. as a result of high background signal from the lipid environment [18]. We can also expect spCryo-LM to assist in solving many dynamic biomolecular structures and dissect the full energy landscape of protein machines.

A naturally emerging exciting avenue of spCryo-LM is a combination with single-particle Cryo-EM. Although these techniques are referred to as 'single-particle' methods, the high-resolution structural information only becomes available after averaging over many particles. In Cryo-EM, several hundreds of individual 2D particle images are averaged to increase the SNR for the classification procedure [176–178] because each image delivers only a small amount of contrast. After aligning, averaging and classification in 2D, in most cases 3D atomic level resolution is achieved from nearly 10–20% of the identified particles as a result of particle heterogeneity or particle damage at the air-water interface [179,180]. As a result, the method still faces challenges in identifying structural heterogeneities caused by mobile domains and intrinsic distributions in assemblies [181–188]. The higher SNR in spCryo-LM, on the other hand, reduces the number of necessary averages by about two orders of magnitude because each 2D projection directly contributes to the 3D reconstruction process. Thus, data from spCryo-LM could massively enhance the yield, reduce error and increase resolution in single-particle Cryo-EM by providing ground truth annotation. In addition to single-particle analysis, high localization precision of fluorescent tags will aid in determining the spatial location of proteins *in situ*, in combination with the rapidly growing field of Cryo-ET [21,102,107,124,189–191]. For this task, however, one has to achieve high labeling densities and tame the background fluorescence, which demands a deeper understanding of the photophysics at CT.

Perspectives

- Cryogenic light microscopy is an emerging high-end technology, which holds great promise in shedding light on the structure of biomolecular entities such as proteins, protein complexes and membrane proteins in their native state within the context of cellular ultrastructure.
- Currently, the method can achieve Angstrom-level resolution for soluble proteins and protein complexes. Work is under way to extend this method to membrane proteins, where other structural biology techniques encounter challenges.

- With a better understanding of the photophysics at CT, it will become possible to conduct *in situ* correlative studies using both light and electron microscope techniques at Angstrom-scale resolution. This will enable the dissection of cellular components and protein structures and will provide unprecedented insight into their physiological roles.

Competing Interests
The authors declare that there are no competing interests associated with the manuscript.

Open Access
Open access for this article was enabled by the participation of Max Planck Digital Library in an all-inclusive *Read & Publish* agreement with Portland Press and the Biochemical Society under a transformative agreement with MPDL.

Acknowledgements
We are grateful to the Max Planck Society for financial support.

Abbreviations
cN_2, cold dry nitrogen; CTs, cryogenic temperatures; Cryo-EM, cryogenic electron microscopy; Cryo-ET, cryogenic electron tomography; Cryo-LM, cryogenic light microscopy; Cryo-PALM, cryogenic photo-activated localization microscopy; FSC, Fourier shell correlation; LHe, liquid helium; LN_2, liquid nitrogen; NA, numerical apertures; PSF, point-spread function; RT, room temperature; SIL, solid-immersion lens; SIM, structured illumination microscopy; SMLM, single-molecule localization microscopy; SNR, signal-to-noise ratio; SR, super-resolution; spCryo-LM, single-particle cryogenic light microscopy.

References
1 Lesk, A.M. (2001) *Introduction to Protein Architecture: the Structural Biology of Proteins*, Oxford University Press, New York
2 Nelson, D.L., Cox, M.M. and Lehninger, A.L. (2017) Lehninger principles of biochemistry
3 Mavroidis, C., Dubey, A. and Yarmush, M.L. (2004) Molecular machines. *Annu. Rev. Biomed. Eng.* **6**, 363–395 https://doi.org/10.1146/annurev.bioeng.6.040803.140143
4 Schliwa, M. and Woehlke, G. (2003) Molecular motors. *Nature* **422**, 759 https://doi.org/10.1038/nature01601
5 Alberts, B. (1998) The cell as a collection of protein machines: preparing the next generation of molecular biologists. *Cell* **92**, 291–294 https://doi.org/10.1016/s0092-8674(00)80922-8
6 Karamanos, T.K. and Clore, G.M. (2022) Large chaperone complexes through the lens of nuclear magnetic resonance spectroscopy. *Annu. Rev. Biophys.* **51**, 223–246 https://doi.org/10.1146/annurev-biophys-090921-120150
7 Fersht, A.R. (2008) From the first protein structures to our current knowledge of protein folding: delights and scepticisms. *Nat. Rev. Mol. Cell Biol.* **9**, 650–654 https://doi.org/10.1038/nrm2446
8 Carpenter, E.P., Beis, K., Cameron, A.D. and Iwata, S. (2008) Overcoming the challenges of membrane protein crystallography. *Curr. Opin. Struct. Biol.* **18**, 581–586 https://doi.org/10.1016/j.sbi.2008.07.001
9 Clore, G.M. and Gronenborn, A.M. (1991) Structures of larger proteins in solution: three- and four-dimensional heteronuclear NMR spectroscopy. *Science* **252**, 1390–1399 https://doi.org/10.1126/science.2047852
10 Wüthrich, K. (1990) Protein structure determination in solution by NMR spectroscopy. *J. Biol. Chem.* **265**, 22059–22062 https://doi.org/10.1016/S0021-9258(18)45665-7
11 Perutz, M.F., Rossmann, M.G., Cullis, A.F., Muirhead, H., Will, G. and North, A.C.T. (1960) Structure of haemoglobin: a three-dimensional Fourier synthesis at 5.5-Å. Resolution, obtained by X-ray analysis. *Nature* **185**, 416–422 https://doi.org/10.1038/185416a0
12 Kendrew, J.C., Bodo, G., Dintzis, H.M., Parrish, R.G., Wyckoff, H. and Phillips, D.C. (1958) A three-dimensional model of the myoglobin molecule obtained by X-ray analysis. *Nature* **181**, 662–666 https://doi.org/10.1038/181662a0
13 Nakane, T., Kotecha, A., Sente, A., McMullan, G., Masiulis, S., Brown, P.M.G.E. et al. (2020) Single-particle cryo-EM at atomic resolution. *Nature* **587**, 152–156 https://doi.org/10.1038/s41586-020-2829-0
14 Cheng, Y., Grigorieff, N., Penczek, P.A. and Walz, T. (2015) A primer to single-particle cryo-electron microscopy. *Cell* **161**, 438–449 https://doi.org/10.1016/j.cell.2015.03.050
15 Kuhlbrandt, W. (2014) The resolution revolution. *Science* **343**, 1443–1444 https://doi.org/10.1126/science.1251652
16 Dubochet, J. (2012) Cryo-EM-the first thirty years. *J. Microsc.* **245**, 221–224 https://doi.org/10.1111/j.1365-2818.2011.03569.x
17 Frank, J. (2006) *Three-Dimensional Electron Microscopy of Macromolecular Assemblies: Visualization of Biological Molecules in Their Native State*, Oxford University Press, New York; online edn, Oxford Academic, 1 Apr. 2010

18 Nygaard, R., Kim, J. and Mancia, F. (2020) Cryo-electron microscopy analysis of small membrane proteins. *Curr. Opin. Struct. Biol.* **64**, 26–33 https://doi.org/10.1016/j.sbi.2020.05.009
19 Wu, M. and Lander, G.C. (2020) How low can we go? Structure determination of small biological complexes using single-particle cryo-EM. *Curr. Opin. Struct. Biol.* **64**, 9–16 https://doi.org/10.1016/j.sbi.2020.05.007
20 Frank, J. (2013) Story in a sample-the potential (and limitations) of cryo-electron microscopy applied to molecular machines. *Biopolymers* **99**, 832–836 https://doi.org/10.1002/bip.22274
21 Hylton, R.K. and Swulius, M.T. (2021) Challenges and triumphs in cryo-electron tomography. *iScience* **24**, 102959 https://doi.org/10.1016/j.isci.2021.102959
22 Lučić, V., Rigort, A. and Baumeister, W. (2013) Cryo-electron tomography: the challenge of doing structural biology *in situ*. *J. Cell Biol.* **202**, 407–419 https://doi.org/10.1083/jcb.201304193
23 Moerner, W.E. and Kador, L. (1989) Optical detection and spectroscopy of single molecules in a solid. *Phys. Rev. Lett.* **62**, 2535–2538 https://doi.org/10.1103/physrevlett.62.2535
24 Orrit, M. and Bernard, J. (1990) Single pentacene molecules detected by fluorescence excitation in a p-terphenyl crystal. *Phys. Rev. Lett.* **65**, 2716–2719 https://doi.org/10.1103/physrevlett.65.2716
25 Lelek, M., Gyparaki, M.T., Beliu, G., Schueder, F., Griffié, J., Manley, S. et al. (2021) Single-molecule localization microscopy. *Nat. Rev. Methods Primers.* **1**, 39 https://doi.org/10.1038/s43586-021-00038-x
26 Betzig, E., Patterson, G.H., Sougrat, R., Lindwasser, O.W., Olenych, S., Bonifacino, J.S. et al. (2006) Imaging intracellular fluorescent proteins at nanometer resolution. *Science* **313**, 1642–1645 https://doi.org/10.1126/science.1127344
27 Rust, M.J., Bates, M. and Zhuang, X. (2006) Sub-diffraction-limit imaging by stochastic optical reconstruction microscopy (STORM). *Nat. Methods* **3**, 793–796 https://doi.org/10.1038/nmeth929
28 Klar, T.A., Jakobs, S., Dyba, M., Egner, A. and Hell, S.W. (2000) Fluorescence microscopy with diffraction resolution barrier broken by stimulated emission. *Proc. Natl Acad. Sci. U.S.A.* **97**, 8206–8210 https://doi.org/10.1073/pnas.97.15.8206
29 Van Oijen, A.M., Köhler, J., Schmidt, J., Müller, M. and Brakenhoff, G.J. (1998) 3-Dimensional super-resolution by spectrally selective imaging. *Chem. Phys. Lett.* **292**, 183–187 https://doi.org/10.1016/s0009-2614(98)00673-3
30 van Oijen, A.M., Köhler, J., Schmidt, J., Müller, M. and Brakenhoff, G.J. (1999) Far-field fluorescence microscopy beyond the diffraction limit. *J. Opt. Soc. Am. A* **16**, 909–915 https://doi.org/10.1364/JOSAA.16.000909
31 Güttler, F., Irngartinger, T., Plakhotnik, T., Renn, A. and Wild, U.P. (1994) Fluorescence microscopy of single molecules. *Chem. Phys. Lett.* **217**, 393–397 https://doi.org/10.1016/0009-2614(94)87003-9
32 Mortensen, K.I., Churchman, L.S., Spudich, J.A. and Flyvbjerg, H. (2010) Optimized localization analysis for single-molecule tracking and super-resolution microscopy. *Nat. Methods* **7**, 377–381 https://doi.org/10.1038/nmeth.1447
33 Pertsinidis, A., Zhang, Y. and Chu, S. (2010) Subnanometre single-molecule localization, registration and distance measurements. *Nature* **466**, 647–651 https://doi.org/10.1038/nature09163
34 Thompson, R.E., Larson, D.R. and Webb, W.W. (2002) Precise nanometer localization analysis for individual fluorescent probes. *Biophys. J.* **82**, 2775–2783 https://doi.org/10.1016/s0006-3495(02)75618-x
35 Gelles, J., Schnapp, B.J. and Sheetz, M.P. (1988) Tracking kinesin-driven movements with nanometre-scale precision. *Nature* **331**, 450–453 https://doi.org/10.1038/331450a0
36 Vicidomini, G., Bianchini, P. and Diaspro, A. (2018) STED super-resolved microscopy. *Nat. Methods* **15**, 173–182 https://doi.org/10.1038/nmeth.4593
37 Sahl, S.J., Hell, S.W. and Jakobs, S. (2017) Fluorescence nanoscopy in cell biology. *Nat. Rev. Mol. Cell Biol.* **18**, 685–701 https://doi.org/10.1038/nrm.2017.71
38 Qu, X., Wu, D., Mets, L. and Scherer, N.F. (2004) Nanometer-localized multiple single-molecule fluorescence microscopy. *Proc. Natl Acad. Sci. U.S.A.* **101**, 11298–11303 https://doi.org/10.1073/pnas.0402155101
39 Gordon, M.P., Ha, T. and Selvin, P.R. (2004) Single-molecule high-resolution imaging with photobleaching. *Proc. Natl Acad. Sci. U.S.A.* **101**, 6462–6465 https://doi.org/10.1073/pnas.0401638101
40 Gustafsson, M.G.L. (2000) Surpassing the lateral resolution limit by a factor of two using structured illumination microscopy. SHORT COMMUNICATION. *J. Microsc.* **198**, 82–87 https://doi.org/10.1046/j.1365-2818.2000.00710.x
41 Betzig, E. (1995) Proposed method for molecular optical imaging. *Opt. Lett.* **20**, 237–239 https://doi.org/10.1364/OL.20.000237
42 Hess, S.T., Girirajan, T.P.K. and Mason, M.D. (2006) Ultra-High resolution imaging by fluorescence photoactivation localization microscopy. *Biophys. J.* **91**, 4258–4272 https://doi.org/10.1529/biophysj.106.091116
43 Heilemann, M., Margeat, E., Kasper, R., Sauer, M. and Tinnefeld, P. (2005) Carbocyanine dyes as efficient reversible single-molecule optical switch. *J. Am. Chem. Soc.* **127**, 3801–3806 https://doi.org/10.1021/ja044686x
44 Patterson, G.H. and Lippincott-Schwartz, J. (2002) A photoactivatable GFP for selective photolabeling of proteins and cells. *Science* **297**, 1873–1877 https://doi.org/10.1126/science.1074952
45 Creemers, T.M.H., Lock, A.J., Subramaniam, V., Jovin, T.M. and Volker, S. (2000) Photophysics and optical switching in green fluorescent protein mutants. *Proc. Natl Acad. Sci. U.S.A.* **97**, 2974–2978 https://doi.org/10.1073/pnas.97.7.2974
46 Sawin, K.E. and Nurse, P. (1997) Photoactivation of green fluorescent protein. *Curr. Biol.* **7**, R606–R607 https://doi.org/10.1016/S0960-9822(06)00313-7
47 Dickson, R.M., Cubitt, A.B., Tsien, R.Y. and Moerner, W.E. (1997) On/off blinking and switching behaviour of single molecules of green fluorescent protein. *Nature* **388**, 355–358 https://doi.org/10.1038/41048
48 Kwon, J., Elgawish, M.S. and Shim, S.H. (2022) Bleaching-resistant super-resolution fluorescence microscopy. *Adv. Sci.* **9**, 2101817 https://doi.org/10.1002/advs.202101817
49 McKinney, S.A., Murphy, C.S., Hazelwood, K.L., Davidson, M.W. and Looger, L.L. (2009) A bright and photostable photoconvertible fluorescent protein. *Nat. Methods* **6**, 131–133 https://doi.org/10.1038/nmeth.1296

50 Shaner, N.C., Lin, M.Z., McKeown, M.R., Steinbach, P.A., Hazelwood, K.L., Davidson, M.W. et al. (2008) Improving the photostability of bright monomeric orange and red fluorescent proteins. *Nat. Methods* **5**, 545–551 https://doi.org/10.1038/nmeth.1209
51 Vogelsang, J., Kasper, R., Steinhauer, C., Person, B., Heilemann, M., Sauer, M. et al. (2008) A reducing and oxidizing system minimizes photobleaching and blinking of fluorescent dyes. *Angew. Chem. Int. Ed. Engl.* **47**, 5465–5469 https://doi.org/10.1002/anie.200801518
52 Aitken, C.E., Marshall, R.A. and Puglisi, J.D. (2008) An oxygen scavenging system for improvement of dye stability in single-molecule fluorescence experiments. *Biophys. J.* **94**, 1826–1835 https://doi.org/10.1529/biophysj.107.117689
53 Rasnik, I., McKinney, S.A. and Ha, T. (2006) Nonblinking and long-lasting single-molecule fluorescence imaging. *Nat. Methods* **3**, 891–893 https://doi.org/10.1038/nmeth934
54 Liu, S., Hoess, P. and Ries, J. (2022) Super-resolution microscopy for structural cell biology. *Annu. Rev. Biophys.* **51**, 301–326 https://doi.org/10.1146/annurev-biophys-102521-112912
55 Helmerich, D.A., Beliu, G., Taban, D., Meub, M., Streit, M., Kuhlemann, A. et al. (2022) Photoswitching fingerprint analysis bypasses the 10-nm resolution barrier. *Nat. Methods* **19**, 986–994 https://doi.org/10.1038/s41592-022-01548-6
56 Legant, W.R., Shao, L., Grimm, J.B., Brown, T.A., Milkie, D.E., Avants, B.B. et al. (2016) High-density three-dimensional localization microscopy across large volumes. *Nat. Methods* **13**, 359–365 https://doi.org/10.1038/nmeth.3797
57 Sauer, M. (2013) Localization microscopy coming of age: from concepts to biological impact. *J. Cell Sci.* **126**, 3505–3513 https://doi.org/10.1242/jcs.123612
58 Shannon, C.E. (1949) Communication in the presence of noise. *Proc. IRE* **37**, 10–21 https://doi.org/10.1109/JRPROC.1949.232969
59 Hettich, C., Schmitt, C., Zitzmann, J., Kühn, S., Gerhardt, I. and Sandoghdar, V. (2002) Nanometer resolution and coherent optical dipole coupling of two individual molecules. *Science* **298**, 385–389 https://doi.org/10.1126/science.1075606
60 Weisenburger, S., Boening, D., Schomburg, B., Giller, K., Becker, S., Griesinger, C. et al. (2017) Cryogenic optical localization provides 3D protein structure data with Angstrom resolution. *Nat. Methods* **14**, 141–144 https://doi.org/10.1038/nmeth.4141
61 Balzarotti, F., Eilers, Y., Gwosch, K.C., Gynnå, A.H., Westphal, V., Stefani, F.D. et al. (2017) Nanometer resolution imaging and tracking of fluorescent molecules with minimal photon fluxes. *Science* **355**, 606–612 https://doi.org/10.1126/science.aak9913
62 Yang, B., Chen, G., Ghafoor, A., Zhang, Y., Zhang, Y., Zhang, Y. et al. (2020) Sub-nanometre resolution in single-molecule photoluminescence imaging. *Nat. Photonics* **14**, 693–699 https://doi.org/10.1038/s41566-020-0677-y
63 Reinhardt, S.C.M., Masullo, L.A., Baudrexel, I., Steen, P.R., Kowalewski, R., Eklund, A.S. et al. (2023) Ångström-resolution fluorescence microscopy. *Nature* **617**, 711–716 https://doi.org/10.1038/s41586-023-05925-9
64 Shaib, A.H., Chouaib, A.A., Chowdhury, R., Mihaylov, D., Zhang, C., Imani, V. et al. (2023) Visualizing proteins by expansion microscopy. *bioRxiv* https://doi.org/10.1101/2022.08.03.502284
65 Sahl, S.J., Matthias, J., Inamdar, K., Khan, T.A., Weber, M., Becker, S. et al. (2023) Direct optical measurement of intra-molecular distances down to the Ångström scale. *bioRxiv* https://doi.org/10.1101/2023.07.07.548133
66 Hurbain, I. and Sachse, M. (2011) The future is cold: cryo-preparation methods for transmission electron microscopy of cells. *Biol. Cell* **103**, 405–420 https://doi.org/10.1042/bc20110015
67 Dubochet, J. (2007) The physics of rapid cooling and its implications for cryoimmobilization of cells. *Methods Cell Biol.* **79**, 7–21 https://doi.org/10.1016/s0091-679x(06)79001-x
68 Korogod, N., Petersen, C.C.H. and Knott, G.W. (2015) Ultrastructural analysis of adult mouse neocortex comparing aldehyde perfusion with cryo fixation. *eLife* **4**, e05793 https://doi.org/10.7554/eLife.05793
69 Weisenburger, S., Jing, B., Renn, A. and Sandoghdar, V. (2013) Cryogenic localization of single molecules with angstrom precision. *Proc. SPIE. Nanoimaging and Nanospectroscopy.* **8815**, 88150D https://doi.org/10.1117/12.2025373
70 Kondo, T., Mutoh, R., Arai, S., Kurisu, G., Oh-Oka, H., Fujiyoshi, S. et al. (2022) Energy transfer fluctuation observed by single-molecule spectroscopy of red-shifted bacteriochlorophyll in the homodimeric photosynthetic reaction center. *J. Chem. Phys.* **156**, 105102 https://doi.org/10.1063/5.0077290
71 Kondo, T., Mutoh, R., Tabe, H., Kurisu, G., Oh-Oka, H., Fujiyoshi, S. et al. (2020) Cryogenic single-molecule spectroscopy of the primary electron acceptor in the photosynthetic reaction center. *J. Phys. Chem. Lett.* **11**, 3980–3986 https://doi.org/10.1021/acs.jpclett.0c00891
72 Kondo, T., Chen, W.J. and Schlau-Cohen, G.S. (2017) Single-molecule fluorescence spectroscopy of photosynthetic systems. *Chem. Rev.* **117**, 860–898 https://doi.org/10.1021/acs.chemrev.6b00195
73 Tietz, C., Chekhlov, O., Dräbenstedt, A., Schuster, J. and Wrachtrup, J. (1999) Spectroscopy on single light-harvesting complexes at low temperature. *J. Phys. Chem. B* **103**, 6328–6333 https://doi.org/10.1021/jp983599m
74 van Oijen, A.M., Ketelaars, M., Köhler, J., Aartsma, T.J. and Schmidt, J. (1999) Unraveling the electronic structure of individual photosynthetic pigment-protein complexes. *Science* **285**, 400–402 https://doi.org/10.1126/science.285.5426.400
75 Van Oijen, A.M., Ketelaars, M., Köhler, J., Aartsma, T.J. and Schmidt, J. (1998) Spectroscopy of single light-harvesting complexes from purple photosynthetic bacteria at 1.2 K. *J. Phys. Chem. B* **102**, 9363–9366 https://doi.org/10.1021/jp9830629
76 Störkel, U., Creemers, T.M.H., Hartog, F.T.H. and Völker, S. (1998) Glass versus protein dynamics at low temperature studied by time-resolved spectral hole burning. *J. Lumin.* **76–77**, 327–330 https://doi.org/10.1016/S0022-2313(97)00287-1
77 Thorn Leeson, D., Wiersma, D.A., Fritsch, K. and Friedrich, J. (1997) The energy landscape of myoglobin: an optical study. *J. Phys. Chem. B* **101**, 6331–6340 https://doi.org/10.1021/jp970908k
78 Ulrich Nienhaus, G., Müller, J.D., McMahon, B.H. and Frauenfelder, H. (1997) Exploring the conformational energy landscape of proteins. *Phys. D Nonlinear Phenom.* **107**, 297–311 https://doi.org/10.1016/S0167-2789(97)00097-3
79 Fritsch, K., Friedrich, J., Parak, F. and Skinner, J.L. (1996) Spectral diffusion and the energy landscape of a protein. *Proc. Natl Acad. Sci. U.S.A.* **93**, 15141–15145 https://doi.org/10.1073/pnas.93.26.15141
80 Leeson, D.T. and Wiersma, D.A. (1995) Looking into the energy landscape of myoglobin. *Nat. Struct. Biol.* **2**, 848–851 https://doi.org/10.1038/nsb1095-848
81 Thorn Leeson, D. and Wiersma, D.A. (1995) Real time observation of low-temperature protein motions. *Phys. Rev. Lett.* **74**, 2138–2141 https://doi.org/10.1103/physrevlett.74.2138
82 Frauenfelder, H., Parak, F. and Young, R.D. (1988) Conformational substates in proteins. *Annu. Rev. Biophys. Biophys. Chem.* **17**, 451–479 https://doi.org/10.1146/annurev.bb.17.060188.002315

83 Mao, B., Tsuda, M., Ebrey, T.G., Akita, H., Balogh-Nair, V. and Nakanishi, K. (1981) Flash photolysis and low temperature photochemistry of bovine rhodopsin with a fixed 11-ene. *Biophys. J.* **35**, 543–546 https://doi.org/10.1016/S0006-3495(81)84809-6
84 Fujiyoshi, S., Hirano, M., Matsushita, M., Iseki, M. and Watanabe, M. (2011) Structural change of a cofactor binding site of flavoprotein detected by single-protein fluorescence spectroscopy at 1.5 K. *Phys. Rev. Lett.* **106**, 078101 https://doi.org/10.1103/physrevlett.106.078101
85 Moerner, W.E. (2010) *Single-Molecule Optical Spectroscopy and Imaging: From Early Steps to Recent Advances*, Springer, Berlin Heidelberg, pp. 25–60
86 Moerner, W.E. and Orrit, M. (1999) Illuminating single molecules in condensed matter. *Science* **283**, 1670–1676 https://doi.org/10.1126/science.283.5408.1670
87 Tabe, H., Sukenobe, K., Kondo, T., Sakurai, A., Maruo, M., Shimauchi, A. et al. (2018) Cryogenic fluorescence localization microscopy of spectrally selected individual FRET pairs in a water matrix. *J. Phys. Chem. B* **122**, 6906–6911 https://doi.org/10.1021/acs.jpcb.8b03977
88 Fujiyoshi, S., Fujiwara, M. and Matsushita, M. (2008) Visible fluorescence spectroscopy of single proteins at liquid-helium temperature. *Phys. Rev. Lett.* **100**, 168101 https://doi.org/10.1103/physrevlett.100.168101
89 Moerner, W.E. (2002) A dozen years of single-molecule spectroscopy in physics, chemistry, and biophysics. *J. Phys. Chem. B* **106**, 910–927 https://doi.org/10.1021/jp012992g
90 Stark, H., Zemlin, F. and Boettcher, C. (1996) Electron radiation damage to protein crystals of bacteriorhodopsin at different temperatures. *Ultramicroscopy* **63**, 75–79 https://doi.org/10.1016/0304-3991(96)00045-9
91 Hulleman, C.N., Li, W., Gregor, I., Rieger, B. and Enderlein, J. (2018) Photon yield enhancement of red fluorophores at cryogenic temperatures. *ChemPhysChem* **19**, 1774–1780 https://doi.org/10.1002/cphc.201800131
92 Furubayashi, T., Motohashi, K., Wakao, K., Matsuda, T., Kii, I., Hosoya, T. et al. (2017) Three-dimensional localization of an individual fluorescent molecule with Angstrom precision. *J. Am. Chem. Soc.* **139**, 8990–8994 https://doi.org/10.1021/jacs.7b03899
93 Li, W.X., Stein, S.C., Gregor, I. and Enderlein, J. (2015) Ultra-stable and versatile widefield cryo-fluorescence microscope for single-molecule localization with sub-nanometer accuracy. *Opt. Express* **23**, 3770–3783 https://doi.org/10.1364/Oe.23.003770
94 Sartori, A., Gatz, R., Beck, F., Rigort, A., Baumeister, W. and Plitzko, J.M. (2007) Correlative microscopy: bridging the gap between fluorescence light microscopy and cryo-electron tomography. *J. Struct. Biol.* **160**, 135–145 https://doi.org/10.1016/j.jsb.2007.07.011
95 Schwartz, C.L., Sarbash, V.I., Ataullakhanov, F.I., McIntosh, J.R. and Nicastro, D. (2007) Cryo-fluorescence microscopy facilitates correlations between light and cryo-electron microscopy and reduces the rate of photobleaching. *J. Microsc.* **227**, 98–109 https://doi.org/10.1111/j.1365-2818.2007.01794.x
96 Agronskaia, A.V., Valentijn, J.A., Van Driel, L.F., Schneijdenberg, C.T.W.M., Humbel, B.M., Van Bergen En Henegouwen, P.M.P. et al. (2008) Integrated fluorescence and transmission electron microscopy. *J. Struct. Biol.* **164**, 183–189 https://doi.org/10.1016/j.jsb.2008.07.003
97 Le Gros, M.A., McDermott, G., Uchida, M., Knoechel, C.G. and Larabell, C.A. (2009) High-aperture cryogenic light microscopy. *J. Microsc.* **235**, 1–8 https://doi.org/10.1111/j.1365-2818.2009.03184.x
98 Kukulski, W., Schorb, M., Welsch, S., Picco, A., Kaksonen, M. and Briggs, J.A.G. (2011) Correlated fluorescence and 3D electron microscopy with high sensitivity and spatial precision. *J. Cell Biol.* **192**, 111–119 https://doi.org/10.1083/jcb.201009037
99 Rigort, A., Bäuerlein, F.J.B., Leis, A., Gruska, M., Hoffmann, C., Laugks, T. et al. (2010) Micromachining tools and correlative approaches for cellular cryo-electron tomography. *J. Struct. Biol.* **172**, 169–179 https://doi.org/10.1016/j.jsb.2010.02.011
100 Schorb, M. and Briggs, J.A.G. (2014) Correlated cryo-fluorescence and cryo-electron microscopy with high spatial precision and improved sensitivity. *Ultramicroscopy* **143**, 24–32 https://doi.org/10.1016/j.ultramic.2013.10.015
101 Li, S., Ji, G., Shi, Y., Klausen, L.H., Niu, T., Wang, S. et al. (2018) High-vacuum optical platform for cryo-CLEM (HOPE): a new solution for non-integrated multiscale correlative light and electron microscopy. *J. Struct. Biol.* **201**, 63–75 https://doi.org/10.1016/j.jsb.2017.11.002
102 Hoffman, D.P., Shtengel, G., Xu, C.S., Campbell, K.R., Freeman, M., Wang, L. et al. (2020) Correlative three-dimensional super-resolution and block-face electron microscopy of whole vitreously frozen cells. *Science* **367**, eaaz5357 https://doi.org/10.1126/science.aaz5357
103 Studer, D., Humbel, B.M. and Chiquet, M. (2008) Electron microscopy of high pressure frozen samples: bridging the gap between cellular ultrastructure and atomic resolution. *Histochem. Cell Biol.* **130**, 877–889 https://doi.org/10.1007/s00418-008-0500-1
104 Dubochet, J., Adrian, M., Chang, J.-J., Homo, J.-C., Lepault, J., McDowall, A.W. et al. (1988) Cryo-electron microscopy of vitrified specimens. *Q. Rev. Biophys.* **21**, 129–228 https://doi.org/10.1017/s0033583500004297
105 Dubochet, J. and McDowall, A.W. (1981) Vitrification of pure water for electron microscopy. *J. Microsc.* **124**, 3–4 https://doi.org/10.1111/j.1365-2818.1981.tb02483.x
106 Huebinger, J., Han, H.-M., Hofnagel, O., Ingrid, P. and Grabenbauer, M. (2016) Direct measurement of water states in cryopreserved cells reveals tolerance toward ice crystallization. *Biophys. J.* **110**, 840–849 https://doi.org/10.1016/j.bpj.2015.09.029
107 Dahlberg, P.D., Saurabh, S., Sartor, A.M., Wang, J., Mitchell, P.G., Chiu, W. et al. (2020) Cryogenic single-molecule fluorescence annotations for electron tomography reveal *in situ* organization of key proteins in Caulobacter. *Proc. Natl Acad. Sci. U.S.A.* **117**, 13937–13944 https://doi.org/10.1073/pnas.2001849117
108 Kaufmann, R., Schellenberger, P., Seiradake, E., Dobbie, I.M., Jones, E.Y., Davis, I. et al. (2014) Super-resolution microscopy using standard fluorescent proteins in intact cells under cryo-conditions. *Nano Lett.* **14**, 4171–4175 https://doi.org/10.1021/nl501870p
109 Chang, Y.-W., Chen, S., Tocheva, E.I., Treuner-Lange, A., Löbach, S., Søgaard-Andersen, L. et al. (2014) Correlated cryogenic photoactivated localization microscopy and cryo-electron tomography. *Nat. Methods* **11**, 737–739 https://doi.org/10.1038/nmeth.2961
110 Briegel, A., Chen, S., Koster, A.J., Plitzko, J.M., Schwartz, C.L. and Jensen, G.J. (2010) Correlated light and electron cryo-microscopy. *Methods Enzymol.* **481**, 317–341 https://doi.org/10.1016/S0076-6879(10)81013-4
111 Hussels, M., Konrad, A. and Brecht, M. (2012) Confocal sample-scanning microscope for single-molecule spectroscopy and microscopy with fast sample exchange at cryogenic temperatures. *Rev. Sci. Instrum.* **83**, 123706 https://doi.org/10.1063/1.4769996
112 Zondervan, R., Kulzer, F., van der Meer, H., Disselhorst, J.A.J.M. and Orrit, M. (2006) Laser-driven microsecond temperature cycles analyzed by fluorescence polarization microscopy. *Biophys. J.* **90**, 2958–2969 https://doi.org/10.1529/biophysj.105.075168
113 Wrigge, G., Gerhardt, I., Hwang, J., Zumofen, G. and Sandoghdar, V. (2008) Efficient coupling of photons to a single molecule and the observation of its resonance fluorescence. *Nat. Phys.* **4**, 60–66 https://doi.org/10.1038/nphys812
114 Yoshita, M., Koyama, K., Hayamizu, Y., Baba, M. and Akiyama, H. (2002) Improved high collection efficiency in fluorescence microscopy with a Weierstrass-Sphere solid immersion lens. *Jpn. J. Appl. Phys.* **41**, L858–L860 https://doi.org/10.1143/jjap.41.l858

115 Tacke, S., Krzyzanek, V., Nusse, H., Wepf, R.A., Klingauf, J. and Reichelt, R. (2016) A versatile high-vacuum cryo-transfer system for cryo-microscopy and analytics. *Biophys. J.* **110**, 758–765 https://doi.org/10.1016/j.bpj.2016.01.024
116 Briegel, A., Ding, H.J., Li, Z., Werner, J., Gitai, Z., Dias, D.P. et al. (2008) Location and architecture of the *Caulobacter crescentus* chemoreceptor array. *Mol. Microbiol.* **69**, 30–41 https://doi.org/10.1111/j.1365-2958.2008.06219.x
117 Dahlberg, P.D. and Moerner, W.E. (2021) Cryogenic super-resolution fluorescence and electron microscopy correlated at the nanoscale. *Annu. Rev. Phys. Chem.* **72**, 253–278 https://doi.org/10.1146/annurev-physchem-090319-051546
118 Wolff, G., Hagen, C., Grünewald, K. and Kaufmann, R. (2016) Towards correlative super-resolution fluorescence and electron cryo-microscopy. *Biol. Cell* **108**, 245–258 https://doi.org/10.1111/boc.201600008
119 Moser, F., Prazak, V., Mordhorst, V., Andrade, D.M., Baker, L.A., Hagen, C. et al. (2019) Cryo-SOFI enabling low-dose super-resolution correlative light and electron cryo-microscopy. *Proc. Natl Acad. Sci. U.S.A.* **116**, 4804–4809 https://doi.org/10.1073/pnas.1810690116
120 Tuijtel, M.W., Koster, A.J., Jakobs, S., Faas, F.G.A. and Sharp, T.H. (2019) Correlative cryo super-resolution light and electron microscopy on mammalian cells using fluorescent proteins. *Sci. Rep.* **9**, 1369 https://doi.org/10.1038/s41598-018-37728-8
121 Sartor, A.M., Dahlberg, P.D., Perez, D. and Moerner, W.E. (2023) Characterization of mApple as a red fluorescent protein for cryogenic single-molecule imaging with turn-off and turn-on active control mechanisms. *J. Phys. Chem. B* **127**, 2690–2700 https://doi.org/10.1021/acs.jpcb.2c08995
122 Mantovanelli, A.M.R., Glushonkov, O., Adam, V., Wulffelé, J., Thédié, D., Byrdin, M. et al. (2023) Photophysical studies at cryogenic temperature reveal a novel photoswitching mechanism of rsEGFP2. *J. Am. Chem. Soc.* **145**, 14636–14646 https://doi.org/10.1021/jacs.3c01500
123 Dahlberg, P.D., Sartor, A.M., Wang, J., Saurabh, S., Shapiro, L. and Moerner, W.E. (2018) Identification of PAmKate as a red photoactivatable fluorescent protein for cryogenic super-resolution imaging. *J. Am. Chem. Soc.* **140**, 12310–12313 https://doi.org/10.1021/jacs.8b05960
124 Liu, B., Xue, Y., Zhao, W., Chen, Y., Fan, C., Gu, L. et al. (2015) Three-dimensional super-resolution protein localization correlated with vitrified cellular context. *Sci. Rep.* **5**, 13017 https://doi.org/10.1038/srep13017
125 Dahlberg, P.D., Perez, D., Hecksel, C.W., Chiu, W. and Moerner, W.E. (2022) Metallic support films reduce optical heating in cryogenic correlative light and electron tomography. *J. Struct. Biol.* **214**, 107901 https://doi.org/10.1016/j.jsb.2022.107901
126 Kaufmann, R., Hagen, C. and Grünewald, K. (2014) Fluorescence cryo-microscopy: current challenges and prospects. *Curr. Opin. Chem. Biol.* **20**, 86–91 https://doi.org/10.1016/j.cbpa.2014.05.007
127 Iancu, C.V., Wright, E.R., Heymann, J.B. and Jensen, G.J. (2006) A comparison of liquid nitrogen and liquid helium as cryogens for electron cryotomography. *J. Struct. Biol.* **153**, 231–240 https://doi.org/10.1016/j.jsb.2005.12.004
128 Pfeil-Gardiner, O., Mills, D.J., Vonck, J. and Kuehlbrandt, W. (2019) A comparative study of single-particle cryo-EM with liquid-nitrogen and liquid-helium cooling. *IUCrJ* **6**, 1099–1105 https://doi.org/10.1107/s2052252519011503
129 Toninelli, C., Gerhardt, I., Clark, A.S., Reserbat-Plantey, A., Götzinger, S., Ristanović, Z. et al. (2021) Single organic molecules for photonic quantum technologies. *Nat. Mater.* **20**, 1615–1628 https://doi.org/10.1038/s41563-021-00987-4
130 Weisenburger, S. (2016) *Cryogenic Super-Resolved Fluorescence Microscopy*, Logos Verlag Berlin GmbH, Berlin
131 Mazal, H., Wieser, F.-F. and Sandoghdar, V. (2022) Deciphering a hexameric protein complex with Angstrom optical resolution. *eLife* **11**, e76308 https://doi.org/10.7554/elife.76308
132 Weisenburger, S., Jing, B., Hänni, D., Reymond, L., Schuler, B., Renn, A. et al. (2014) Cryogenic colocalization microscopy for nanometer-distance measurements. *ChemPhysChem* **15**, 763–770 https://doi.org/10.1002/cphc.201301080
133 Nahmani, M., Lanahan, C., Derosier, D. and Turrigiano, G.G. (2017) High-numerical-aperture cryogenic light microscopy for increased precision of superresolution reconstructions. *Proc. Natl Acad. Sci. U.S.A.* **114**, 3832–3836 https://doi.org/10.1073/pnas.1618206114
134 Xu, X., Xue, Y., Tian, B., Feng, F., Gu, L., Li, W. et al. (2018) Ultra-stable super-resolution fluorescence cryo-microscopy for correlative light and electron cryo-microscopy. *Sci. China Life Sci.* **61**, 1312–1319 https://doi.org/10.1007/s11427-018-9380-3
135 Furubayashi, T., Ishida, K., Kashida, H., Nakata, E., Morii, T., Matsushita, M. et al. (2019) Nanometer accuracy in cryogenic far-field localization microscopy of individual molecules. *J. Phys. Chem. Lett.* **10**, 5841–5846 https://doi.org/10.1021/acs.jpclett.9b02184
136 Wang, L., Bateman, B., Zanetti-Domingues, L.C., Moores, A.N., Astbury, S., Spindloe, C. et al. (2019) Solid immersion microscopy images cells under cryogenic conditions with 12 nm resolution. *Commun. Biol.* **2**, 74 https://doi.org/10.1038/s42003-019-0317-6
137 Phillips, M.A., Harkiolaki, M., Susano Pinto, D.M., Parton, R.M., Palanca, A., Garcia-Moreno, M. et al. (2020) CryoSIM: super-resolution 3D structured illumination cryogenic fluorescence microscopy for correlated ultrastructural imaging. *Optica* **7**, 802–812 https://doi.org/10.1364/OPTICA.393203
138 Sexton, D.L., Burgold, S., Schertel, A. and Tocheva, E.I. (2022) Super-resolution confocal cryo-CLEM with cryo-FIB milling for *in situ* imaging of deinococcus radiodurans. *Curr. Res. Struct. Biol.* **4**, 1–9 https://doi.org/10.1016/j.crstbi.2021.12.001
139 Kirchweger, P., Mullick, D., Swain, P.P., Wolf, S.G. and Elbaum, M. (2023) Correlating cryo-super resolution radial fluctuations and dual-axis cryo-scanning transmission electron tomography to bridge the light-electron resolution gap. *J. Struct. Biol.* **215**, 107982 https://doi.org/10.1016/j.jsb.2023.107982
140 Trautman, J.K., Macklin, J.J., Brus, L.E. and Betzig, E. (1994) Near-field spectroscopy of single molecules at room temperature. *Nature* **369**, 40–42 https://doi.org/10.1038/369040a0
141 Ambrose, W.P., Goodwin, P.M., Keller, R.A. and Martin, J.C. (1994) Alterations of single molecule fluorescence lifetimes in near-field optical microscopy. *Science* **265**, 364–367 https://doi.org/10.1126/science.265.5170.364
142 Ambrose, W.P. and Moerner, W.E. (1991) Fluorescence spectroscopy and spectral diffusion of single impurity molecules in a crystal. *Nature* **349**, 225–227 https://doi.org/10.1038/349225a0
143 Orlov, S.V., Naumov, A.V., Vainer, Y.G. and Kador, L. (2012) Spectrally resolved analysis of fluorescence blinking of single dye molecules in polymers at low temperatures. *J. Chem. Phys.* **137**, 194903 https://doi.org/10.1063/1.4766321
144 Suzuki, K., Habuchi, S. and Vacha, M. (2011) Blinking of single dye molecules in a polymer matrix is correlated with free volume in polymers. *Chem. Phys. Lett.* **505**, 157–160 https://doi.org/10.1016/j.cplett.2011.02.041
145 Sluss, D., Bingham, C., Burr, M., Bott, E.D., Riley, E.A. and Reid, P.J. (2009) Temperature-dependent fluorescence intermittency for single molecules of violamine R in poly(vinyl alcohol). *J. Mater. Chem.* **19**, 7561 https://doi.org/10.1039/b909076b
146 Hoogenboom, J.P., Hernando, J., Van Dijk, E.M.H.P., Van Hulst, N.F. and García-Parajó, M.F. (2007) Power-law blinking in the fluorescence of single organic molecules. *Chemphyschem* **8**, 823–833 https://doi.org/10.1002/cphc.200600783

147 Clifford, J.N., Bell, T.D.M., Tinnefeld, P., Heilemann, M., Melnikov, S.M., Hotta, J.-I. et al. (2007) Fluorescence of single molecules in polymer films: sensitivity of blinking to local environment. *J. Phys. Chem. B* **111**, 6987–6991 https://doi.org/10.1021/jp072864d
148 Yeow, E.K.L., Melnikov, S.M., Bell, T.D.M., De Schryver, F.C. and Hofkens, J. (2006) Characterizing the fluorescence intermittency and photobleaching kinetics of dye molecules immobilized on a glass surface. *J. Phys. Chem. A* **110**, 1726–1734 https://doi.org/10.1021/jp055496r
149 Schuster, J., Cichos, F. and Von Borczyskowski, C. (2005) Influence of self-trapped states on the fluorescence intermittency of single molecules. *Appl. Phys. Lett.* **87**, 051915 https://doi.org/10.1063/1.2006217
150 Hoogenboom, J.P., Van Dijk, E.M.H.P., Hernando, J., Van Hulst, N.F. and García-Parajó, M.F. (2005) Power-law-distributed dark states are the main pathway for photobleaching of single organic molecules. *Phys. Rev. Lett.* **95**, 097401 https://doi.org/10.1103/physrevlett.95.097401
151 Kozankiewicz, B. and Orrit, M. (2014) Single-molecule photophysics, from cryogenic to ambient conditions. *Chem. Soc. Rev.* **43**, 1029–1043 https://doi.org/10.1039/c3cs60165j
152 Böning, D., Wieser, F.-F. and Sandoghdar, V. (2021) Polarization-encoded colocalization microscopy at cryogenic temperatures. *ACS Photonics* **8**, 194–201 https://doi.org/10.1021/acsphotonics.0c01201
153 Wieser, F.-F. (2023) *Single-particle Cryogenic Light Microscopy*, Max Placnk Institute for the Science of Light& Friedrich-Alexander-Universitat, PhD Thesis, 129 p, Erlangen, Germany
154 Renn, A., Seelig, J. and Sandoghdar, V. (2006) Oxygen-dependent photochemistry of fluorescent dyes studied at the single molecule level. *Mol. Phys.* **104**, 409–414 https://doi.org/10.1080/00268970500361861
155 Zondervan, R., Kulzer, F., Orlinskii, S.B. and Orrit, M. (2003) Photoblinking of rhodamine 6G in poly(vinyl alcohol): radical dark state formed through the triplet. *J. Phys. Chem. A* **107**, 6770–6776 https://doi.org/10.1021/jp034723r
156 Dvornek, N.C., Sigworth, F.J. and Tagare, H.D. (2015) SubspaceEM: a fast maximum-a-posteriori algorithm for cryo-EM single particle reconstruction. *J. Struct. Biol.* **190**, 200–214 https://doi.org/10.1016/j.jsb.2015.03.009
157 Nieuwenhuizen, R.P.J., Lidke, K.A., Bates, M., Puig, D.L., Grünwald, D., Stallinga, S. et al. (2013) Measuring image resolution in optical nanoscopy. *Nat. Methods* **10**, 557–562 https://doi.org/10.1038/nmeth.2448
158 Harauz, G. and van Heel, M. (1986) Exact filters for general geometry three dimensional reconstruction. *Optik* **73**, 146–156
159 Van Heel, M. and Schatz, M. (2005) Fourier shell correlation threshold criteria. *J. Struct. Biol.* **151**, 250–262 https://doi.org/10.1016/j.jsb.2005.05.009
160 Heydarian, H., Joosten, M., Przybylski, A., Schueder, F., Jungmann, R., Werkhoven, B.V. et al. (2021) 3D particle averaging and detection of macromolecular symmetry in localization microscopy. *Nat. Commun.* **12**, 2847 https://doi.org/10.1038/s41467-021-22006-5
161 Huijben, T.A.P.M., Heydarian, H., Auer, A., Schueder, F., Jungmann, R., Stallinga, S. et al. (2021) Detecting structural heterogeneity in single-molecule localization microscopy data. *Nat. Commun.* **12**, 3791 https://doi.org/10.1038/s41467-021-24106-8
162 Curd, A.P., Leng, J., Hughes, R.E., Cleasby, A.J., Rogers, B., Trinh, C.H. et al. (2021) Nanoscale pattern extraction from relative positions of sparse 3D localizations. *Nano Lett.* **21**, 1213–1220 https://doi.org/10.1021/acs.nanolett.0c03332
163 Bates, M. (2018) Single-particle analysis for fluorescence nanoscopy. *Nat. Methods* **15**, 771–772 https://doi.org/10.1038/s41592-018-0151-7
164 Sieben, C., Banterle, N., Douglass, K.M., Gönczy, P. and Manley, S. (2018) Multicolor single-particle reconstruction of protein complexes. *Nat. Methods* **15**, 777–780 https://doi.org/10.1038/s41592-018-0140-x
165 Salas, D., Le Gall, A., Fiche, J.-B., Valeri, A., Ke, Y., Bron, P. et al. (2017) Angular reconstitution-based 3D reconstructions of nanomolecular structures from superresolution light-microscopy images. *Proc. Natl Acad. Sci. U.S.A.* **114**, 9273–9278 https://doi.org/10.1073/pnas.1704908114
166 Heydarian, H., Schueder, F., Strauss, M.T., Van Werkhoven, B., Fazel, M., Lidke, K.A. et al. (2018) Template-free 2D particle fusion in localization microscopy. *Nat. Methods* **15**, 781–784 https://doi.org/10.1038/s41592-018-0136-6
167 Mulhall, E.M., Gharpure, A., Lee, R.M., Dubin, A.E., Aaron, J.S., Marshall, K.L. et al. (2023) Direct observation of the conformational states of PIEZO1. *Nature* **620**, 1117–1125 https://doi.org/10.1038/s41586-023-06427-4
168 Molle, J., Jakob, L., Bohlen, J., Raab, M., Tinnefeld, P. and Grohmann, D. (2018) Towards structural biology with super-resolution microscopy. *Nanoscale* **10**, 16416–16424 https://doi.org/10.1039/c8nr03361g
169 Lerner, E., Cordes, T., Ingargiola, A., Alhadid, Y., Chung, S., Michalet, X. et al. (2018) Toward dynamic structural biology: two decades of single-molecule Förster resonance energy transfer. *Science* **359**, eaan1133 https://doi.org/10.1126/science.aan1133
170 Strack, R. (2019) Deep learning in imaging. *Nat. Methods* **16**, 17–17 https://doi.org/10.1038/s41592-018-0267-9
171 Dahmardeh, M., Mirzaalian Dastjerdi, H., Mazal, H., Köstler, H. and Sandoghdar, V. (2023) Self-supervised machine learning pushes the sensitivity limit in label-free detection of single proteins below 10 kDa. *Nat. Methods* **20**, 442–447 https://doi.org/10.1038/s41592-023-01778-2
172 Piccoli, S., Suku, E., Garonzi, M. and Giorgetti, A. (2013) Genome-wide membrane protein structure prediction. *Curr. Genomics* **14**, 324–329 https://doi.org/10.2174/13892029113149990009
173 Hisham Mazal, F.F.W., Bollschweiler, D., Schambony, A. and Sandoghdar, V. (2023) Resolving membrane protein structures in their near-native environment with Angstrom optical resolution. In preparation
174 Tao, X., Zhao, C. and Mackinnon, R. (2023) Membrane protein isolation and structure determination in cell-derived membrane vesicles. *Proc. Natl Acad. Sci. U.S.A.* **120**, e2302325120 https://doi.org/10.1073/pnas.2302325120
175 Heuser, J. (2000) The production of 'cell cortices' for light and electron microscopy. *Traffic* **1**, 545–552 https://doi.org/10.1034/j.1600-0854.2000.010704.x
176 Noble, A.J., Dandey, V.P., Wei, H., Brasch, J., Chase, J., Acharya, P. et al. (2018) Routine single particle CryoEM sample and grid characterization by tomography. *eLife* **7**, e34257 https://doi.org/10.7554/eLife.34257
177 Cheng, Y. (2015) Single-particle cryo-EM at crystallographic resolution. *Cell* **161**, 450–457 https://doi.org/10.1016/j.cell.2015.03.049
178 Scheres, S.H.W. (2010) Classification of structural heterogeneity by maximum-likelihood methods. *Methods Enzymol.* **482**, 295–320 https://doi.org/10.1016/S0076-6879(10)82012-9
179 Rosenthal, P.B. and Henderson, R. (2003) Optimal determination of particle orientation, absolute hand, and contrast loss in single-particle electron cryomicroscopy. *J. Mol. Biol.* **333**, 721–745 https://doi.org/10.1016/j.jmb.2003.07.013
180 D'Imprima, E. and Kühlbrandt, W. (2021) Current limitations to high-resolution structure determination by single-particle cryoEM. *Q. Rev. Biophys.* **54**, e4 https://doi.org/10.1017/s0033583521000020
181 Papai, G., Frechard, A., Kolesnikova, O., Crucifix, C., Schultz, P. and Ben-Shem, A. (2020) Structure of SAGA and mechanism of TBP deposition on gene promoters. *Nature* **577**, 711–716 https://doi.org/10.1038/s41586-020-1944-2

182 Grisshammer, R. (2020) The quest for high-resolution G protein-coupled receptor–G protein structures. *Proc. Natl Acad. Sci. U.S.A.* **117**, 6971–6973 https://doi.org/10.1073/pnas.2002665117
183 Nwanochie, E. and Uversky, V.N. (2019) Structure determination by single-particle cryo-electron microscopy: only the sky (and intrinsic disorder) is the limit. *Int. J. Mol. Sci.* **20**, 4186 https://doi.org/10.3390/ijms20174186
184 Serna, M. (2019) Hands on methods for high resolution cryo-electron microscopy structures of heterogeneous macromolecular complexes. *Front. Mol. Biosci.* **6**, 33 https://doi.org/10.3389/fmolb.2019.00033
185 Scheres, S.H.W. (2016) Processing of structurally heterogeneous cryo-EM data in RELION. *Methods Enzymol.* **579**, 125–157 https://doi.org/10.1016/bs.mie.2016.04.012
186 Scheres, S.H.W., Gao, H., Valle, M., Herman, G.T., Eggermont, P.P.B., Frank, J. et al. (2007) Disentangling conformational states of macromolecules in 3D-EM through likelihood optimization. *Nat. Methods* **4**, 27–29 https://doi.org/10.1038/nmeth992
187 Orlova, E.V. and Saibil, H.R. (2004) Structure determination of macromolecular assemblies by single-particle analysis of cryo-electron micrographs. *Curr. Opin. Struct. Biol.* **14**, 584–590 https://doi.org/10.1016/j.sbi.2004.08.004
188 Guo, Y.R. and MacKinnon, R. (2017) Structure-based membrane dome mechanism for Piezo mechanosensitivity. *eLife* **6**, e33660 https://doi.org/10.7554/eLife.33660
189 Wu, G.-H., Mitchell, P.G., Galaz-Montoya, J.G., Hecksel, C.W., Sontag, E.M., Gangadharan, V. et al. (2020) Multi-scale 3D cryo-correlative microscopy for vitrified cells. *Structure* **28**, 1231–1237.e1233 https://doi.org/10.1016/j.str.2020.07.017
190 Li, W., Lu, J., Xiao, K., Zhou, M., Li, Y., Zhang, X. et al. (2023) Integrated multimodality microscope for accurate and efficient target-guided cryo-lamellae preparation. *Nat. Methods* **20**, 268–275 https://doi.org/10.1038/s41592-022-01749-z
191 Berger, C., Premaraj, N., Ravelli, R.B.G., Knoops, K., López-Iglesias, C. and Peters, P.J. (2023) Cryo-electron tomography on focused ion beam lamellae transforms structural cell biology. *Nat. Methods* **20**, 499–511 https://doi.org/10.1038/s41592-023-01783-5